NERC Scientific Facilities and Technology Ion Microprobe Facility

University of Edinburgh
NERC Ion Microprobe Facility

2013 Annual Science Report

Ion Microprobe Facility
School of Geosciences
Kings Buildings
West Mains Road
Edinburgh
EH9 3JW

http://www.geos.ed.ac.uk/facilities/

Contents

Ion Microprobe Projects

Snapshots of Climate Variability in the Southern Tropical Pacific

N. Allison[1], A.W. Tudhope[2]

[1]School of Geography and Geosciences, University of St. Andrews, St. Andrews KY16 9AL, UK
[2]School of Geosciences, University of Edinburgh, Edinburgh, EH9 3JW, UK

The tropical Pacific plays a key role in global climate variability and change, being a prime source of heat driving major components of atmospheric circulation and the hydrological cycle. Accurate reconstruction of past sea surface temperatures (SSTs) in the this region is is crucial to help develop our understanding of the drivers and mechanisms of climate change, and to enable us to accurately predict future climate. Here we used SIMS to determine Sr/Ca in several fossil massive Porites spp. coral skeletons, collected from the Great Barrier Reef (GBR), during IODP expedition 325. Our aim was to use skeletal Sr/Ca to reconstruct past sea surface temperatures in the GBR. The fossil specimens are well preserved but contain minor amounts of secondary aragonite cements which could significantly affect the Sr/Ca composition of the skeleton if analysed by bulk i.e. by drilling samples along the growth axis of the coral. Secondary aragonite cements contain higher Sr/Ca than the surrounding primary coral and bias reconstructed SSTs to cooler values [1]. The high spatial resolution of SIMS analysis (typically ≤30 μm) allows the analysis of the pristine primary coral structures independent of any secondary cement.

Results

We measured Sr/Ca along short transects (spanning ~2 years) of one modern and three fossil specimens with ages ranging from 10.4 ky to 13.1 ky. We planned to analyse 2 other *Porites* spp. specimens with estimated ages of ~24 and 33 ky. However one of these specimens had been mis-identified and was not a *Porites* spp. and the other was subsequently dated as only 13.1 ky. Sample Sr/Ca data from the modern coral and one fossil are shown in Figure 1. SIMS indicates that the skeletal Sr/Ca in pristine massive *Porites* spp. corals is dominated by weekly-monthly oscillations, which exceed the magnitude of seasonal variations observed in drilled samples [2]. These short term oscillations do not reflect SST but probably reflect variations in biological processes in the coral tissue. In spite of this, credible SST records can be obtained from Porites spp. coral skeletons by smoothing multiple SIMS analyses at ~2 monthly resolution and minimizing the effects of short-period high frequency biological noise [2].
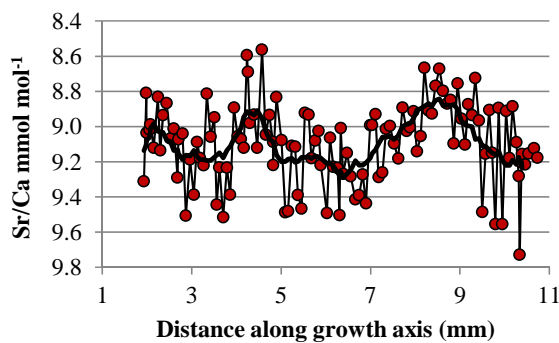
Figure 1. SIMS Sr/Ca measurements across transects of 2 Porites spp skeletons. Each transect spans ~ 2 years of skeletal growth. To the left is a fossil transect (dated at 12.769 ky) and below is a transect across a modern massive Porites spp. collected from Myrmidon Reef, GBR. Precision (2σ) of individual analyses is smaller that the symbols. A smoothed, ~2 month Sr/Ca running mean is shown by thick black line in each case.
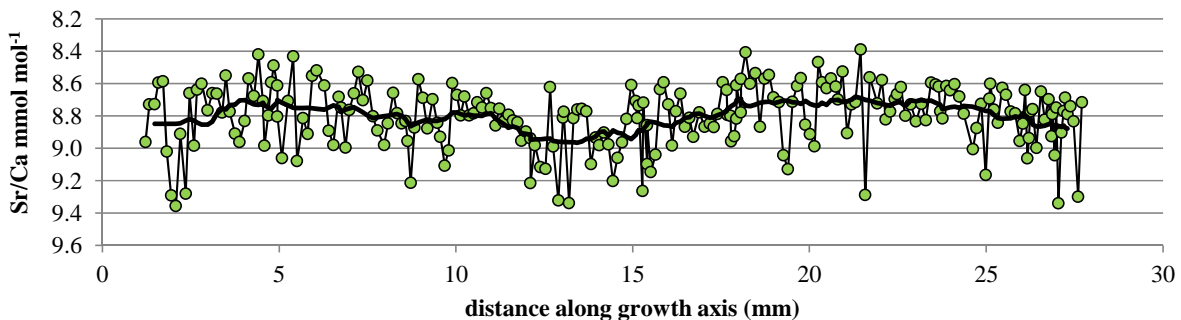
Table 1. Mean skeletal Sr/Ca and reconstructed sea surface temperature (SST) of a 2 year transect of each coral studied. Sr/Ca errors are 95% confidence limits of multiple SIMS analyses and SST errors are calculated from this analytical precision.

Coral age (years)	Sr/Ca (mmol mol^{-1})	Reconstructed SST (°C)
Modern	8.86 ± 0.026	26.8
10402	9.16 ± 0.046	21.5 ± 0.8
12769	9.17 ± 0.038	21.3 ± 0.6
13146	9.12 ± 0.038	22.2 ± 0.6

We observed similar Sr/Ca oscillations in both the modern coral and fossil specimens. The preservation of these oscillations in the geochemistry of the primary coral structures in the fossil corals supports our interpretation that these structures are diagenetically unaltered.

Mean skeletal Sr/Ca data of the two year transects of each coral are summarised in Table1. Sr/Ca was significantly higher in each of the fossil corals compared to the modern specimen. The temperature sensitivity of Sr/Ca in massive *Porites* corals from the GBR is ~0.06 mmol mol^{-1} °C^{-1} and on this basis the skeletal Sr/Ca data suggest that SSTs were ~5°C cooler at 10.4 to 13.1 ky compared to the present day. However skeletal Sr/Ca and coral calcification (or skeletal extension) rate are inversely correlated in corals and we note that the skeletal linear extension rates in the fossil corals (typically 4-6 mm y^{-1}) are less than half those observed in the modern coral (typically 14 mm y^{-1}). Variations in skeletal Sr/Ca between colonies of different growth rates can equate to errors in reconstructed SST of up to ~3°C [3] and we cannot rule out the possibility that varying skeletal growth rate affected skeletal Sr/Ca and depressed reconstructed SSTs to anomalously cool values.

We are currently working to identify an independent skeletal tracer to enable us to correct coral Sr/Ca for variations in calcification rate. We propose to apply this tracer to the GBR Sr/Ca dataset in the future to enable us to accurately interpret the SST signal encoded in the coral skeletons.

References
[1] N. Allison et al. (2007), Palaeoenvironmental records from fossil corals: the effects of submarine diagenesis on temperature and climate estimates, Geochim. Cosmochim. Acta , 71, 4693- 4703.
[2] N. Allison et al. (2005) Reconstruction of deglacial sea surface temperatures in the tropical Pacific from selective analysis of a fossil coral, Geophys. Res. Lett., 32, L17609, doi: 10.1029/2005GL023183.
[3] N.F. Goodkin et al. (2007) A multicoral calibration method to approximate a universal equation relating Sr/Ca and growth rate to sea surface temperature, Paleoceanography, 22, PA1214.

Channelized Fluid Flow and Eclogite-facies Metasomatism along the Subduction Shear Zone

S.Angiboust[1], T. Pettke[2], CJ De Hoog[3], B. Caron[4] & O. Oncken[1]

[1] Geoforschungszentrum (Gfz) Potsdam D-14473, Germany
[2] Institute of Geological Sciences, Bern Ch-3012, Switzerland
[3] School of Geosciences, University Of Edinburgh, Edinburgh EH9 3JW, UK
[4] Institut Des Sciences De La Terre De Paris, UPMC Paris 75252, France

In order to better understand and characterize the signature of subduction zone fluids, we studied some metasomatic rinds formed around eclogite blocks in a serpentinite shear zone from the Monviso ophiolite (W. Alps; 550°C, 2.5 GPa). Bulk rock and trace element analysis (bulk and LA-ICPMS) demonstrate that these eclogites underwent a significant enrichment in Cr, Mg and Ni during eclogite-facies metasomatism. Some of these blocks also show a minor enrichment in Large Ion Lithophile Elements (LILEs) as visible by the growth of high-pressure phengite within metasomatic rinds. These two observations indicate that the metasomatic overprint is dominated by a serpentinite-signature with some minor contributions from sediments and/or altered oceanic crust, which are generally considered as a source for LILE enrichment. It is important to constrain the source of the fluids responsible for this metasomatic enrichment to know whether prograde serpentinite dehydration could have caused the observed metasomatism here. According to recent studies [1], such fluids should carry a heavy $\delta^{11}B$ signature (+15 to +25 permil).

We therefore decided to make *in situ* characterization of the Boron isotope signature ($\delta^{11}B$) of metasomatic minerals using the Ion Microprobe Facility at the Edinburgh University. Our measurements revealed that metasomatic minerals formed within this shear zone (phengite, chlorite, clinopyroxene) exhibit relatively light signatures, comprised between -5 and +5 permil, which is much lighter than inferred serpentinite breakdown signatures (Figure 1). Analysis of antigorite (High Temperature polymorph of serpentinite) $\delta^{11}B$ signature from the adjacent non-metasomatized serpentinites yielded similar values (0 to +5 permil). This result, in line with trace-element characterization, shows that fluids responsible for metasomatism were derived from the surrounding serpentinite.
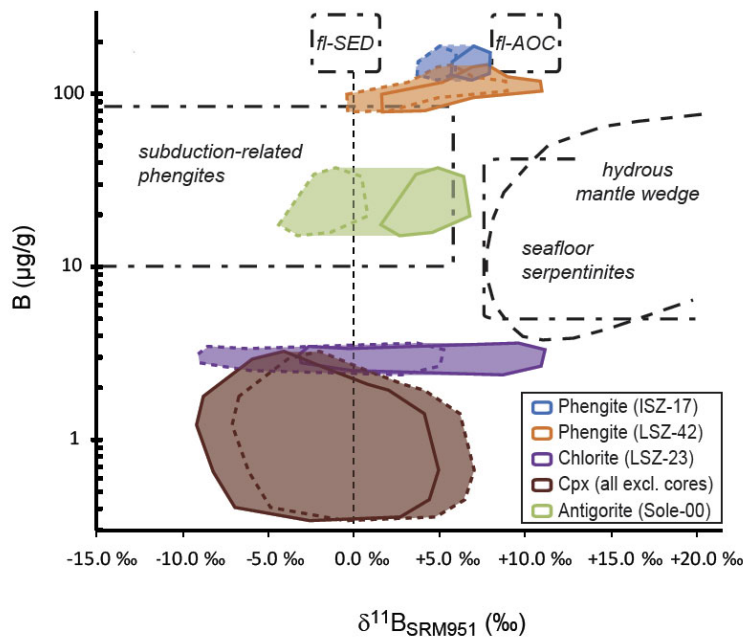
Figure 1: Synthesis of obtained B isotopic data. Dotted coloured domains indicate bulk data and plain colour domains indicate matrix-corrected data. Typical fluid composition and concentration for shallow-depth sediment (fl-SED) and shallow-depth AOC signature (fl-AOC) are plotted versus typical serpentinite and subduction phengite signatures

Given the high amount of fluids needed to explain these metasomatic features and given the absence of major dehydration textures in surrounding serpentinites, we conclude that fluids wetting block surfaces derived from the deeper antigorite breakdown, which is the only source of fluids susceptible to provide large amounts of fluids at such depths (>80 km). This implies that fluids were able to migrate from antigorite dehydration depths (~120km) to Monviso eclogites depths (~80km) along the subduction shear zone (Figure 2). While slab components of diverse flavour have long been recognized to be central in triggering island arc magmatism, this example is among the first to document synkinematic, long-range, large-scale, channelized dehydration fluid flow within subducted oceanic slabs (manuscript accepted for publication in Journal of Petrology).
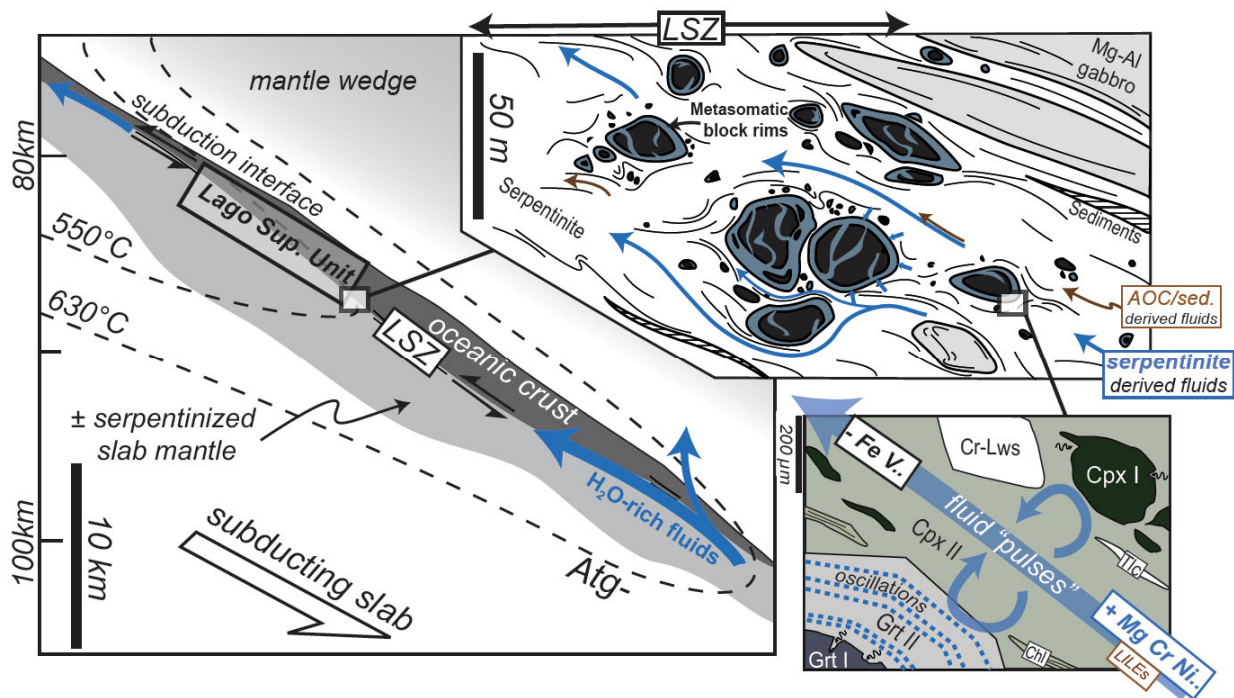
Figure 2: Schematic view of the Lower Shear Zone in Monviso ophiolite showing fluid transfer pathways (blue arrows) within the slab at different scales: along the shear zone forming along the base of the crust (left), around and between the tectonic blocks in the LSZ (upper right corner) and through eclogite matrix within metasomatically recrystallized block rims (lower right corner). Blue circular arrows in inset represent chemical interaction between the aqueous fluid phase and growing minerals. A likely but moderate contribution to the geochemical signal from fluids equilibrated with sediments (and/or altered oceanic crust –AOC-) is represented by the brown arrow.

References

[1] M. Scambelluri and S. Tonarini (2012) Geology **40**, 907-910.

Magma Storage Conditions and Magmatic Volatile Budget of Nabro Volcano, Eritrea

Jon Blundy[1] and Amy Donovan[2]

1 School of Earth Sciences, University of Bristol, Bristol BS8 1RJ, UK
2 Department of Geography, University of Cambridge, Cambridge CB2 3EN

Scientific report

Nabro volcano in Eritrea erupted in June 2011 for the first time in recorded history, producing lava flows of trachybasalt to trachybasalatic andesite and significant emission of SO_2. Nabro is a large stratovolcano with a summit caldera, breached to the south west. It forms part of the Bidu massif [1], which is an alignment running NW-SE between the Red Sea and the main Afar spreading centre. Prior to 2011, very little research had been done at Nabro. Our study represents the first comprehensive analysis of eruptive products and processes at this remote volcano. A particular objective was to characterise the volatile burden of the erupted magma.

In October 2011, a NERC-funded Urgency Grant allowed sampling of the lavas and tephras from the 2011 eruption. We have analysed 90 melt inclusions from 11 tephra samples to constrain the volatile budget of the eruption. Melt inclusions from both plagioclase and olivine were identified and analysed using the 1270 ion probe for CO_2 and light elements, and the 4f for H_2O, light elements and heavy trace elements. In addition to work at the IMF, electron probe analysis was carried out for major elements, S, Cl and F at the University of Cambridge and these data used for ion-yield normalisation.

The melt inclusion volatile data are shown in Figure 1, along with isobars calculated using the model of Papale et al. [2]. However, based on volatile-trace element systematics (i.e. increasing CO_2 and H_2O with increasing incompatible trace elements) some of the more primitive inclusions appear to be volatile-undersaturated, suggesting that the isobars in Figure 1 are minima. The overall evolution is consistent with crystallisation that is initially undersaturated in volatiles and subsequently evolves by a combination of closed system degassing and crystallisation.
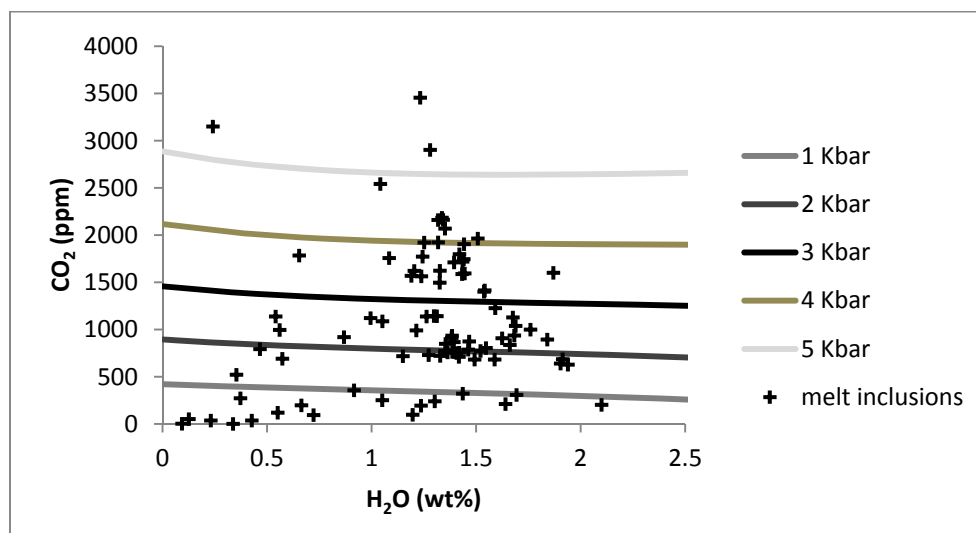
Figure 1. Volatile contents of melt inclusions from the 2011 eruption of Nabro.

The model of Papale et al. [2] suggests that there are clusters of inclusions at pressures between 2-3 kbar corresponding to depth to the storage region of between 5 and 10 km, which is consistent with

both experimental data (A. Donovan, unpublished) and seismology (J. Hamlyn, pers. comm.). We estimate the original water content of the magma at ~1.2 wt%, which is higher than other volcanoes in the Afar region. The highest saturation pressures (>5 kbar) are suggestive of lower crustal or near-Moho depths

In addition to the volatile measurements, we analysed the trace element compositions for 60 melt inclusions. Figure 2 shows the REE composition of the melt inclusions, normalised to primitive mantle [3]. The high level of enrichment in LREE is also unusual in Afar. In general, the melt inclusions and whole rock data obtained by XRF suggest that Nabro is more alkaline, wetter and possibly has a deeper source than other rocks in the Afar region.
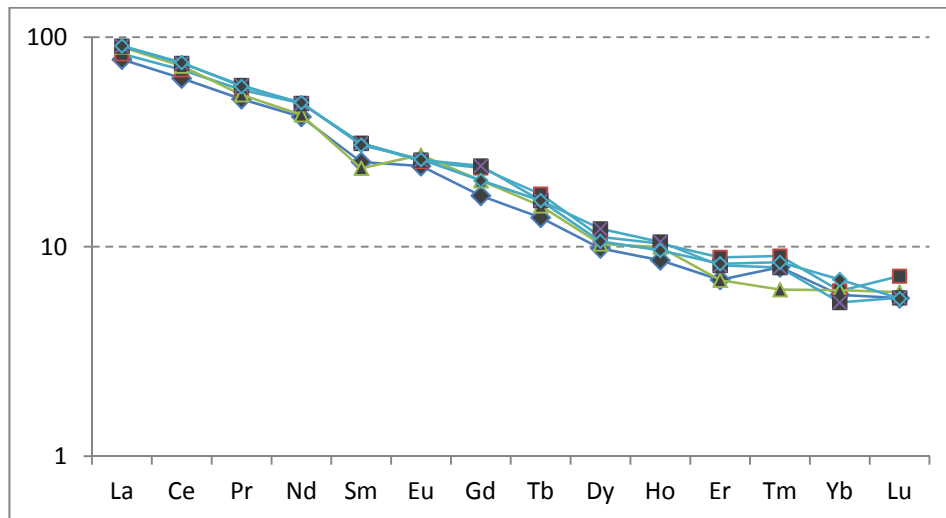
Figure 2. Representative PUM-normalised REE compositions of Nabro melt inclusions.

We have compared the rocks from Nabro with published data from the literature. It is plausible that Nabro and Dubbi volcano are sourced from the same magma supply, and that basalts from the Edd volcanic field [4] represent parental magmas from this source.

Summary

Our results show that the main magma chamber supplying the 2011 eruption of Nabro was at 5-10km depth, and that the magma is relatively wet for the Afar region, with ~1.2 wt% water and ~3500 ppm CO_2 in the most primitive inclusions. These inclusions are also very deep in origin – approximately 20km depth (according to the model of Papale et al. [2]), which is consistent with the base of the crust in the region. They are enriched in LREE, and may originate from a large magma source that also supplies Dubbi and Edd volcanoes, at the edge of the Danakil horst.

References

[1] Wiart, P., & Oppenheimer, C. (2005). Large magnitude silicic volcanism in north Afar: The Nabro Volcanic Range and Ma'alalta volcano. *Bulletin of Volcanology*, *67*(2), 99-115.
[2] Papale, P., Moretti, R., & Barbato, D. (2006). The compositional dependence of the saturation surface of $H_2O + CO_2$ fluids in silicate melts. *Chemical Geology*, *229*(1), 78-95.
[3] Sun, S. S., & McDonough, W. (1989). Chemical and isotopic systematics of oceanic basalts: implications for mantle composition and processes. *Geological Society, London, Special Publications*, *42*(1), 313-345.
[4] De Fino, M., La Volpe, L., & Lirer, L. (1978). Geology and volcanology of the Edd-Bahar Assoli area (Ethiopia). *Bulletin Volcanologique*, *41*(1), 32-42.

Hydrogen Mobility in Olivine under Mantle Conditions

J. Brooke & G. Bromiley

School of GeoSciences, University of Edinburgh, Edinburgh EH9 3JW, UK

It has been established that the majority of nominally anhydrous minerals (NAMs) can incorporate water in the form of structurally bound hydrogen and that, as a result, there may be a significant volume of water stored in the Earth's mantle (estimates range from almost none to several ocean volumes). This water could play a key role in the geodynamics of the Earth's interior and quantifying the amount of water in mantle minerals is therefore an important step in understanding many deep-Earth processes. However, the deep Earth is clearly not an accessible area of study and models of the interior structure of the planet are primarily based on geochemical and geophysical considerations, as well as analysis of what samples are available. The water content of the mantle can be estimated through the analysis of MORB, OIB and xenolith material but these estimates may not be representative of the whole mantle as MORB/OIB samples typically derive from shallow depths and there is significant potential for modification of water content during xenolith ascent.

As hydrogen is highly mobile (due to fast diffusion rates) it acts as the dominant charge-carrying species in mantle minerals and, consequently, electrical conductivity is particularly sensitive to even small changes in water content. It is therefore possible to use geophysical techniques such as magnetotellurics (MT) to 'map-out' the water content of the mantle although accurate interpretation of such data relies on good quality conductivity data from mineral physics studies. Difficulties in measuring conductivity in wet (hydrogen-bearing) samples, coupled with the fact that traditional diffusion experiments do not provide thermodynamic data on hydrogen mobility, mean that the influence of hydrogen on conductivity remains poorly constrained - with different groups of researchers in different laboratories obtaining calculated mantle reservoir water contents that differ by as much as several orders of magnitude (e.g. [1], [2]).

A novel experimental design has been proposed to investigate electrical conductivity in synthetic hydrous olivine by considering hydrogen-deuterium exchange in single crystals. Hydrogen-saturated crystals synthesised under mantle conditions are sealed in a gold capsule with deuterium oxide,
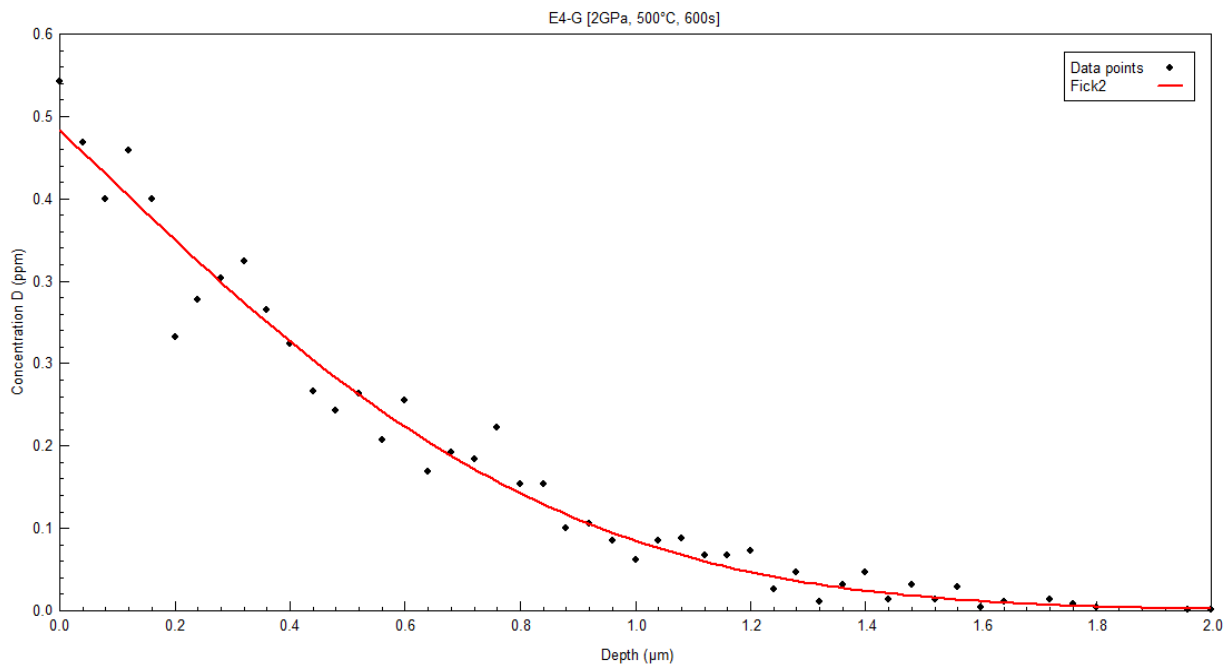
Figure 1. Analysis points for E4-G (Fo$_{100}$, synthesised at 2GPa, 1200°C; D-H exchange at 2GPa, 500°C for 600 seconds) showing a good fit to Fick's second law of diffusion (red line).

allowing deuterium to exchange with hydrogen under controlled pressure and temperature conditions for a specified time period (theoretically determined based on published diffusion rates). The resulting H-D exchange profiles can be characterised using SIMS and fitted to Fick's law; extrapolated diffusion data for hydrogen self mobility can then be directly related to electrical conductivity through the Nernst-Einstein equation.

A one-day pilot SIMS study was used to evaluate a series of preliminary experimental runs and obtain initial results, and the resulting diffusion profiles show a close fit to Fick's law (Figure 1). Further steps in data analysis rely on accurate determination of the depth of the profile (not carried out during the pilot study), although estimates yield approximate diffusion coefficients that are in line with published values for olivine.

In addition, the pilot-study demonstrated that the grown crystal faces were not always satisfactorily flat to allow for precise analysis, as no polishing is undertaken at the sample preparation stage (analysis relies on depth profiles and polishing would remove the top surface). An additional step of polishing synthesised crystals prior to D-H exchange has been incorporated into the final experimental procedure.

References

[1] T. Yoshino et al. (2006) Nature **443**, 973-976
[2] D. Wang et al. (2006) Nature **443**, 977-980

K-Ca Dating of Low-Temperature Alteration (K-Feldspar) of the Uppermost Oceanic Crust

L.A. Coogan and R.H. Hinton

School of Earth and Ocean Sciences, University of Victoria, Victoria, Canada

Introduction

The alteration of the upper oceanic crust (the basaltic lava sequence) in low temperature (10's of Celsius), off-axis, hydrothermal systems plays a major role in global geochemical cycles. We have recently been investigating the feedback played by this system on the long-term carbon cycle [1,2]. One of the key uncertainties in this is how soon after crustal formation alteration and chemical exchange with the oceans occurs. Previous studies of the timing of alteration have used either: (i) comparison of the Sr-isotopic composition of secondary minerals with the seawater Sr-isotopic curve to estimate the minerals age of formation; or (ii) isochrons through different phases commonly separated from different samples (e.g. clays, carbonates and zeolites from different veins). The former approach has substantial uncertainty due to the incorporation of basaltic Sr into hydrothermal fluids. The latter approach relies on alteration occurring synchronously for all phases and the data are generally inconsistent with this at least in detail. To address this issue we have been developing an approach to use K-Ca dating of secondary K-feldspar to directly date the alteration of the upper oceanic crust.

K-feldspar in the upper oceanic crust

Potassium feldspar occurs as a secondary phase that forms in low-temperature, off-axis, hydrothermal systems largely replacing plagioclase either in the groundmass or phenocrysts commonly associated with calcite (Fig. 1) and beidellite (a cation-poor clay). It is more common in crust of Cretaceous age [2] for unknown reasons but likely related to differences in ocean temperature and composition.

500 μm
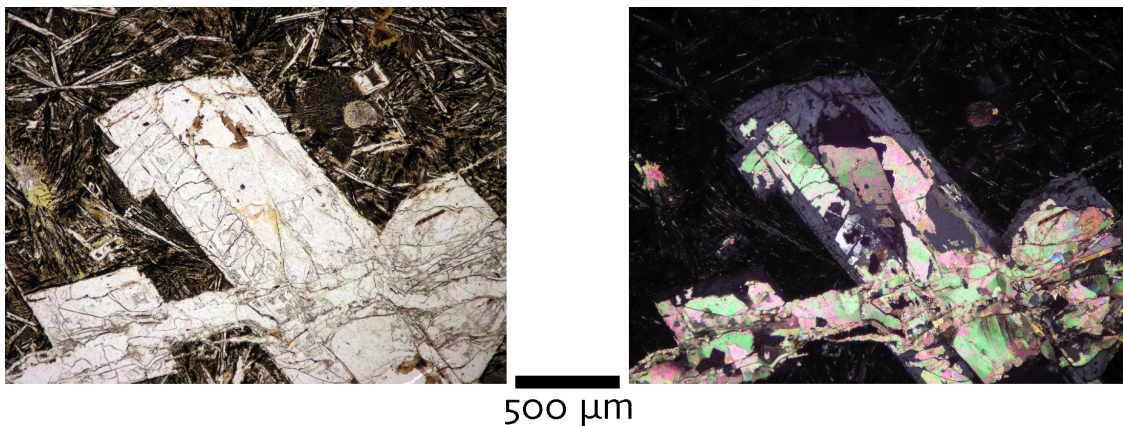
Figure 1. Typical texture for K-feldspar in altered oceanic lavas. K-feldspar and calcite replace both phenocrysts and microlites of plagioclase. K-feldspar is the low birefringence phase.

Analytical approach

Potassium-calcium (^{40}K-^{40}Ca) dating of K-feldspar (90% of ^{40}K decays to ^{40}Ca with only 10% decaying to the more commonly discussed daughter product ^{40}Ar) has the potential to provide a powerful way to determine the timing of seafloor K-metasomatism. The approach we are using broadly follows the methodology of Harrison et al. [3] in using doubly charged ions to suppress isobaric interference of ^{40}K on ^{40}Ca due to the orders of magnitude lower ion yields for doubly charge alkalis than for Ca [4]. Because there is very little oceanic crust older than Cretaceous in age this approach is analytically challenging due to the limited radiogenic Ca production. A key to successful dating using this approach is to analyse material with low unradiogenic Ca contents. We used the Cameca IMS 1270 for these analyses using an O primary beam and a single detector and peak hoping between ^{39}K^{++}, ^{40}Ca^{++}, ^{42}Ca^{++}, ^{44}Ca^{++} as well as ^{29}Si$^+$ and ^{41}K$^+$.

Glass K-spar standards

To help in the calibration we prepared a series of glass standards from spec-pure materials of near K-feldspar composition doped with different levels of Ca (from a single element trace element standard). This solution was analysed by double-spike MC-ICP-MS to ensure it had a natural isotopic composition (it does; $^{40}Ca/^{44}Ca$ = 47.1544). Electron microprobe analyses show these are homogeneous in terms of major elements (Table 1). Ion probe analyses of these and other feldspar standards show that, contrary to expectations, there is a slight bias in favour of the heavy isotope. For example, forty analyses of the lowest Ca standard glass gave an average $^{40}Ca/^{44}Ca$ = 46.9 and eight analyses of the higher Ca standards gave an average $^{40}Ca/^{44}Ca$ = 46.75. We are currently investigating the origin of this unexpectedly low measured $^{40}Ca/^{44}Ca$ (e.g. drift, interference, etc).

	SiO_2	Al_2O_3	FeO	Na_2O	K_2O	Total	Nominal Ca (ppm)
Kspar-glass-1	68.82	17.42	0.22	0.36	11.48	98.35	0
Kspar-glass-2	68.81	17.20	0.17	0.18	11.87	98.28	111
Kspar-glass-3	68.46	17.18	0.20	0.29	12.04	98.22	202

Table 1: Major element composition of glass standards prepared as part of this study. Modified from perfect K-feldspar stoichiometry to lower the melting point sufficiently to ensure complete homogenization.

Results

Until we have resolved the issues around the sub-natural $^{40}Ca/^{44}Ca$ measured in the standards we cannot process the data into ages. However, we do see a clearly elevation of $^{40}Ca/^{44}Ca$ in the lowest Ca crystals indicating that the radiogenic contribution can be determined and that meaningful ages will be resolvable (Fig. 2).
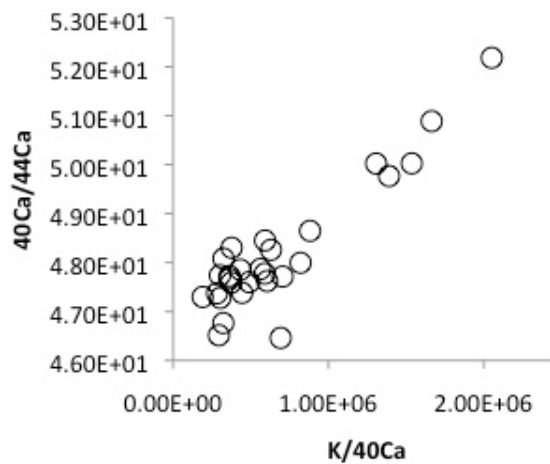
Figure 2. Example of clear contribution of radiogenic ^{40}Ca to the $^{40}Ca/^{44}Ca$ in low Ca (high K/Ca) K-feldspar.

References

[1] Gillis and Coogan, (2011) Earth and Planetary Science Letters **302** 385-392
[2] Coogan and Gillis, (2013) G-cubed **14** 1771-1786
[3] T.M. Harrison et al., (2010) Earth and Planetary Science Letters **299** 426-433
[4] R.W. Hinton, (1990) Chemical Geology **83**, 11-25

Trace Metal Constraints on Coccolithophore Calcification Mechanisms

T. Dunkley Jones[1] & K. Prentice[2]

[1]School of Geography, Earth and Environmental Sciences, University of Birmingham, B15 2TT, UK
[2]Department of Earth Science and Engineering, Imperial College, London, SW7 2AZ, UK

Rationale:

Coccolithophores, single-celled haptophyte algae, are a dominant group of modern oceanic phytoplankton. Their ability to biomineralize complex polycrystalline particles of calcite, known as coccoliths, together with their great abundance and geographic spread makes them a major component of the oceanic carbon/carbonate cycle. There is growing concern about the response of coccolithophore calcification to the effects of anthropogenic ocean acidification, with potential impacts on oceanic carbonate production, changes in mineral ballasting and the effectiveness of the biological pump, as well as the resilience of coccolithophore species to changes in ocean pH. The fundamental pathways of calcification, including whether biomineralization occurs inside or outside of the coccolithophore cell, are however, still unknown for some of the major calcifying groups in the modern plankton that have not yet been successfully grown in culture experiments. Of particular interest is the biomineralization of the characteristic pentagonal liths of the somewhat enigmatic genera *Braarudosphaera* (Figure 1).

This project aims to develop and apply a novel approach to investigating whether modern and ancient coccolithophore species biomineralize calcium carbonate inside or outside of the coccolithophore cell.

We propose to use a new methodology to identify intra- versus extra-cellular calcification based on the trace metal concentrations of coccolith calcite. Simply put, the more standard mechanism of intra-cellular calcification, which has been directly observed in culture in a number of species, appears to be highly discriminating against the inclusion of magnesium ions into coccolith calcite but allows for the inclusion of strontium to varying degrees, such that cocclith calcite is typically depleted in Mg and enriched in Sr compared to calcite forming in equilibrium with surrounding sea water. In contrast, if certain non-standard coccolith types are calcifying outside of the cell wall, then trace metals are not subject to transport through the same cellular ion channels to the site of biomineralization and are thus likely to be closer in trace metal composition to calcite in equilibrium with the surrounding sea water, i.e. show higher Mg and lower Sr concentrations.
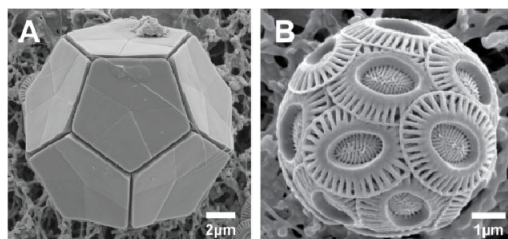
Figure 1: *Pentalith (*B. bigelowii*) and placolith (*E. huxleyi*) morphologies. Note layered coccoliths in* E. huxleyi *resulting from repeated exocytosis of new coccoliths through the cell membrane to form the lower layers. The interlocking, non-layered structure of* B. bigelowii *implies calcification of pentaliths close to their final position. Courtesy of J. Young.*

Methods:

Braarudosphaera bigelowii is a prime target for testing whether extra-cellular calcification produces a distinct trace metal geochemical signal to that of standard placolith coccoliths formed inside the cell. If the trace element concentrations of *Braarudosphaera* are distinct, and fall closer to values expected from calcification in equilibrium with seawater, this is both strong support for an extra-cellular calcification mechanism for *Braarudosphaera* pentaliths and provides a population of trace element values typical for extra cellular calcification that can be compared both to other extant coccoliths with ambiguous calcification mechanisms, most notably holococcoliths, and the fossil record.

Our methodology follows that used very successfully in previous analyses undertaken on cocoliths at the NERC IMF facility using a simple stew of microfiltered coccolith assemblages pressed into indium stubs. A copper TEM grid pressed into the indium stub is used to map suitable specimens using SEM

before analysis at the IM facility and makes relocation of samples relatively simple with the probe optics and Ca mapping. Specimens are subject to a short ~90 second sputter using a high current beam to clean away surface contaminants and then analysed with a high-resolution (<5 μm), low current (0.015nA) beam over 20 cycles. The stability of trace element counts through the analysis cycle and the counts of Al are monitored to check for surficial contamination.

Results:

Pilot data for this proposal clearly indicate that there is a large phylogenetic control, typically at family to ordinal level, on coccolith Sr/Ca (Figure 2). This can result in significant offsets in both the Sr/Ca and Mg/Ca ratios between coccoliths of different species from within a single fossil assemblage. Further, this pilot data indicates that major trace metal variations between coccolithophore clades are related to the mode of coccolith biomineralization. This is most marked for the Braarudosphaeraceae (Figure 2).

Three results of this pilot data inform our research objectives. First placolith chemistry appears to be relatively invariant both through time, from the middle Eocene to modern, ***and*** between species of the dominant Cenozoic placolith-forming coccolithophore families at any given interval. All placoliths analysed have characteristic low Mg/Ca ratios and Sr/Ca between ~2 to 4mmol mol^{-1}. Second, pentaliths of the Braarudosphaeraceae have Mg/Ca ratios consistently one to two orders of magnitude greater, and Sr/Ca ratios lower, than contemporaneous placoliths. Unlike the placoliths, there is also a clear shift in pentalith chemistry through time, with middle Eocene (~42Ma) pentaliths having both Sr/Ca and Mg/Ca ratios of less than a third of modern and late Oligocene forms.
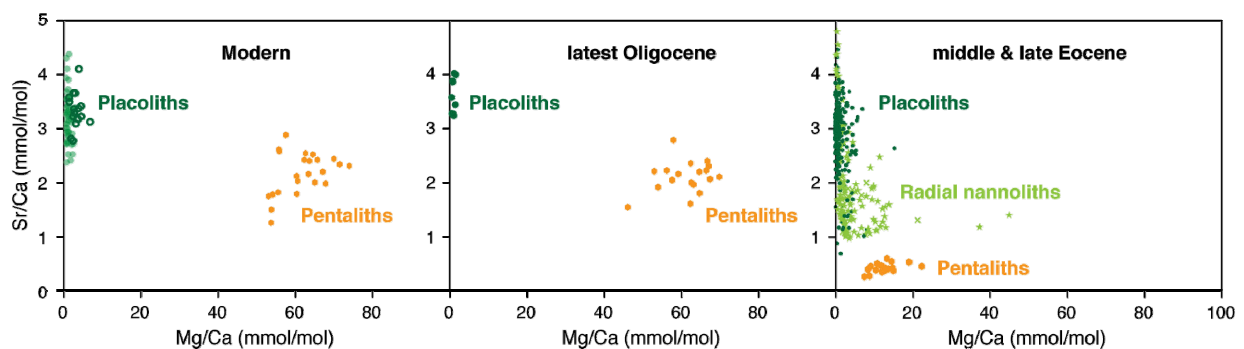
Figure 2: *Sr/Ca and Mg/Ca compositions of Cenozoic coccolith groups. Note relatively stable placolith chemistry through time and major shift in braarudosphaerid pentalith geochemistry from middle Eocene to latest Oligocene samples. Modern placoliths:* C. pelagicus, E. huxleyi *(open circles); latest Oligocene,* R. bisecta*; middle & late Eocene;* C. pelagicus, C. formosus, R. bisecta, R. dictyoda*. Radial nannoliths;* Discoaster saipanensis, D. tanii *and* Sphenolithus moriformis*. Modern and latest Oligocene pentaliths* B. bigelowii*; Eocene pentaliths* P. papillatum.

Finally, the Eocene radial nannoliths, dominantly discoasters, also show distinct trace element chemistry to both the placoliths and the pentaliths (Figure 2). Although closer to, and in part overlapping with the placolith population, discoasters trace element compositions range from specimens with high Sr/Ca values (>3.5 mmol mol^{-1}) and very low Mg/Ca ratios to a significant proportion of the population (~40%) with Sr/Ca ratios lower than typical placoliths (<2 mmol mol^{-1}) but with higher Mg/Ca ratios (~5-15 mmol mol^{-1}). Constraining the trace element chemistry of the discoasters, its variability in different nutrient regimes and its response to changing seawater chemistry is critical for the interpretation of many Cenozoic fine-fraction trace metal records as the discoasters are major components of pre-Pliocene tropical carbonate oozes.

Insights into Volcanic Processes from Water in the Structure of Pyroxenes

M. Edmonds[1], S. Kohn[2] & Edinburgh Ion Microprobe Facility[3]

[1]Earth Sciences, University of Cambridge, CB2 3EQ, UK
[2]Earth Sciences, University of Bristol, Bristol BS8 1RJ, UK
[3]School of GeoSciences, University of Edinburgh, Edinburgh EH9 3JW, UK

Introduction

Water in arc magmas influences profoundly petrogenesis, crustal assimilation, magma buoyancy, compressibility, rheology, eruption style, and the availability of fluids for metal transport and deposition. Records of magma water content are elusive and poorly constrained. Melt inclusions are subject to re-equilibration, post-entrapment processes and are in themselves a biased record, only forming during conditions of rapid crystal growth. In this study we seek to establish whether useful records of magma water content are stored in volcanic phenocrysts of pyroxene.

Strategy

Phenocrysts of augite and enstatite were picked from crushed fractions of samples from a number of different volcanic centres. The samples were all scoria or pumice, chosen to minimise the effect of water loss from the phenocrysts. Crystals were polished, or double polished, then mounted in indium for H_2O analysis using Secondary Ion Mass Spectrometry (SIMS) at the University of Edinburgh. Backgrounds for H_2O in pyroxene were ~ 5-8 ppm. Crystals were then analysed for major elements using electron microprobe at Cambridge. Double polished crystals were analysed for their H_2O content by Fourier Transform Infra red Spectroscopy. Melt inclusions hosted within the crystals were also analysed for H_2O (using SIMS) and major elements (using electron microprobe).
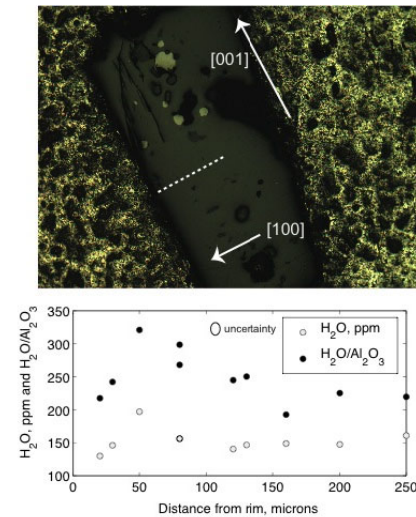
Figure 1. Top, reflected light image of a pyroxene crystal (approximately 2 mm long) mounted in indium for analysis, with crystallographic directions and the location of the analytical traverse marked. Bottom, H_2O concentration and H_2O/Al_2O_3 along a traverse through the crystal.

Results and discussion

The H_2O content of pyroxenes ranges from 50-300 ppm (**Figures 1, 2, 3**) and is correlated with Al and Mg in the Soufriere Hills Volcano pumice (**Figure 2**). In a small subset of grains there is a decrease in H_2O content towards the rim of the crystal (**Figure 1**), but on the whole the there is little relationship between distance from the rim and H_2O content (**Figure 2, left**).
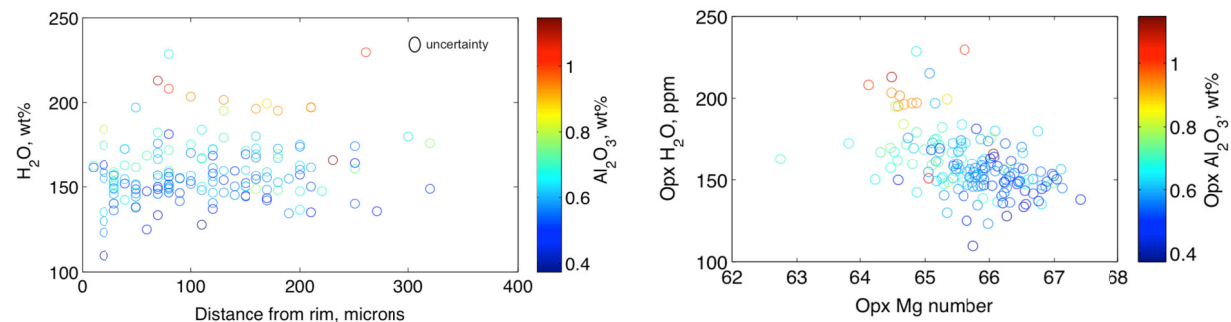
Figure 2. H_2O content of orthopyroxenes from Soufriere Hills Volcano pumice (from SIMS) plotted against left, distance from crystal rim and right, the Mg number of the orthopyroxene. In both plots the data points are colour-coded for orthopyroxene Al_2O_3 content.

These data show that most of the grains have not lost H_2O by diffusion during magma ascent to lower pressures, when the surrounding melt would have outgassed H_2O.

The H_2O content of pyroxenes varies between the volcanoes studied, with the pyroxenes from Pantelleria (aegirine augite) containing both the least Al and the least H_2O (**Figure 3**), despite the melt inclusions containing up to 3 wt% H_2O (**Figure 4**). Pyroxenes from Soufriere Hills and South Soufriere Hills contain the most H_2O, with melt inclusions containing up to around 6 wt% H_2O. (**Figure 4**).
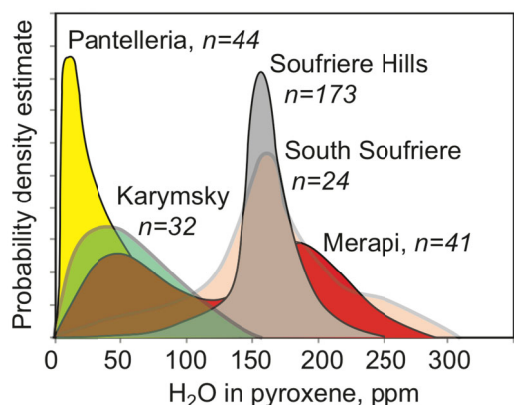
In general, there appears to be a linear relationship between the H_2O content of melt inclusions and the H_2O content of the host crystal (**Figure 3**), although there is considerable scatter.

Figure 3. Probability density estimates to show the H_2O content of pyroxenes from a range of volcanic centres: Pantelleria (Italy), Karymsky (Russia), Soufriere Hills and South Soufriere Hills (Montserrat) and Merapi (Indonesia). *n* is the number of crystals analysed.

The pyroxene-melt partition coefficients range from 0.00064 for the very Al-poor Pantelleria pyroxenes, to 0.0080 for the Al-rich Merapi pyroxenes (**Figure 4**). These values are similar to, although slightly lower than, partition coefficients reported in the literature for synthetic pyroxenes [1, 2].
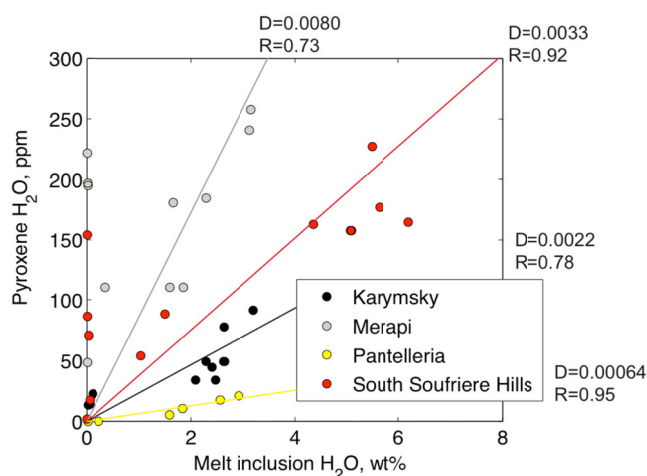
Figure 4. Pyroxene H_2O content plotted against the H_2O content of the melt inclusions hosted by the same crystal. Regressions through the data for each sample yield an estimate for the pyroxene-melt partition coefficient, D. The R value is the Pearson correlation coefficient.

References
[1] S.C. Kohn and K.J. Grant (2006) Reviews in Mineralogy and Geochemistry **62**, 231-241.
[2] K.J. Grant, S.C. Kohn, R.A. Brooker (2006). Contributions to Mineralogy and Petrology **151**, 651-664.

Inclusions in Accessory Minerals: Source Tracers?

M. Fowler[1], E. Bruand[1] & C. Storey[1]

[1] School of Earth and Environmental Sciences, University of Portsmouth, Portsmouth PO1 3QL, UK

Introduction

Accessory minerals hosting rare earth elements (REE; e.g. zircon, apatite, titanite, allanite) represent a low modal proportion of igneous rocks but often dominate the REE budget. They are therefore important in petrogenetic studies, particularly in granites and related rocks in which they may be particularly abundant [1]. Further, if shown to be a reliable indicator of source magma composition, the elemental signature of accessory minerals and inclusions (especially those armoured in zircon) may provide a new tool to understand the secular evolution of the magmatic record and its response to the development of plate tectonics [2], via the investigation of detrital heavy mineral accumulations. Previous trace element work with matrix apatite and titanite has suggested that these minerals are particularly informative [3-8]. While the utility of zircon in this regard is still debated [3,9] , apatite inclusions within zircon have also been shown to give insight into the whole rock chemistry of a granite [6,10]. In associated work using LA-ICPMS [8], the analysis of discrete accessory minerals has allowed partial reconstruction of the crystallization processes and history of two plutons, and highlights one aspect that was not apparent in the whole rock data. New results reported here, on apatite inclusions within zircon and titanite, are shown also to give access to: (i) part of the crystallization history, and (ii) the whole rock chemistry by simple application of mineral-melt distribution coefficients. The subject plutons are high Ba-Sr granites, chosen for their comparability with sanukitoids [11] but undeformed and not reworked, unlike many Archaean sanukitoid examples.

Results

Images of the different accessory phases (Fig.1) reveal that both titanite and zircon contain apatite inclusions. These are present from the core to the outer rim of the crystals and have been analysed using the the Cameca ims 4f at the Edinburgh Ion Microprobe Facility. Results obtained on apatite inclusions (within titanite or zircon) show that Sr and Ce/Y correlate with apatite composition from the matrix (Fig. 2).
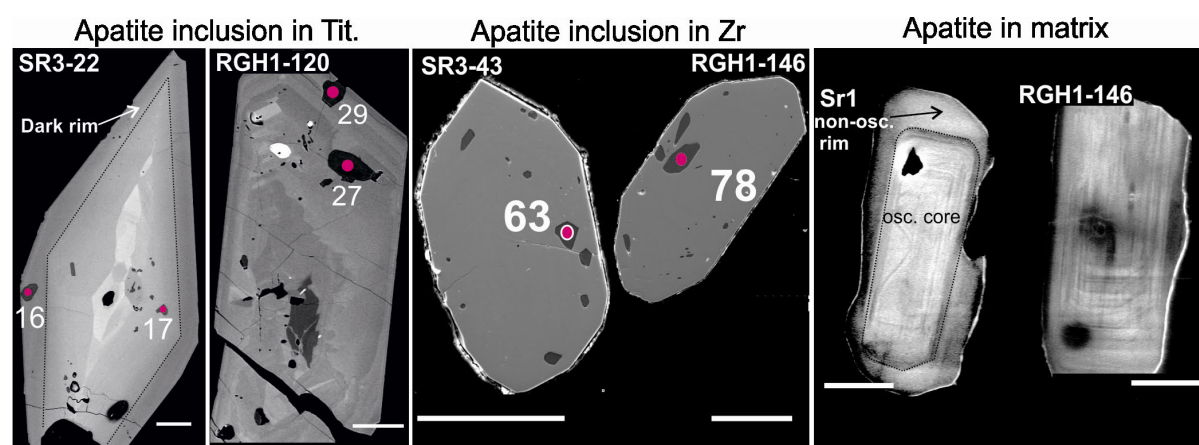
Figure 1. Titanite, zircon and apatite crystals from the matrix in Strontian and Rogart localities. Representative analyses of apatite inclusions in zircon and titanite are labelled with numbers corresponding to data analysis obtained by ionprobe. The scale corresponds to 100 μm.
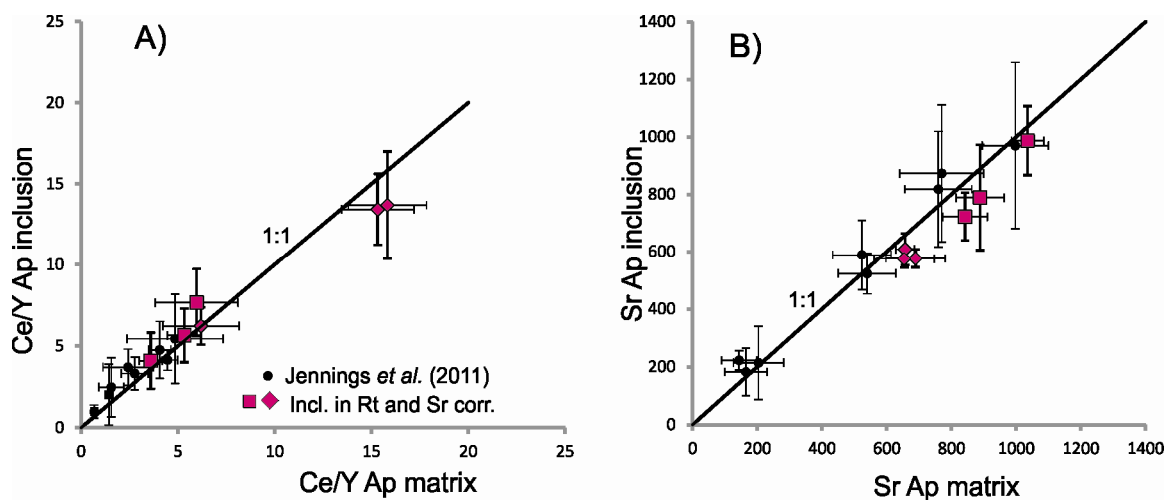
Figure 2. A) 1:1 correlation between Ce/Y in apatite inclusions and Ce/Y in apatite from the matrix. Grey symbols associated with bold error bars are data corrected from Cl-richer apatite group. B) 1:1 correlation between Sr content in apatite inclusions and from the matrix.

These new results confirm that first findings by [6] are applicable to samples from other magmatic suites. Further, apatite inclusion trace-element compositions within titanite from Strontian vary corresponding to their locations within the host crystal (core or rim). Such variations record a mixing event at Strontian (between granitoid magma and a late influx of mafic magma) which was not identified using whole rock data. Local mixing features between the granitoids and the local appinite and microdiorite (mafic rocks) can be observed at the outcrop scale. In samples from Rogart, where there is less field evidence of interaction with mafic magmas, results suggest that titanite and apatite only record in-situ crystal fractionation. Therefore, following work on the Rogart and Strontian plutons [8], the new results show that it is possible to reconstruct part of the crystallisation history of a pluton by using a combination of titanite and apatite compositions *within in a single host grain*.

Future work

The ion probe data briefly described above form part of the NERC-funded project "When on Earth did modern plate tectonics begin?" (NE/I025573/1). They support the critical challenge of the project, which is to establish elemental and/or isotopic fingerprints that adequately distinguish between accessory minerals with TTG, sanukitoid and BADR parentage. A proof-of-concept source attribution study of detrital minerals from well-constrained river catchments and appropriate clastic sediments (e.g. Torridonian sediments draining the Lewisian basement) is planned for this summer.

References

[1] Gromet and Silver (1983) Geochimica and Cosmochimica Acta **47**, 925-939
[2] Martin et al. (2005) Lithos **79**, 1-24
[3] Hoskin et al. (2000) Journal of Petrology **41**, 1365-1396
[4] Chu et al. (2009) Journal of Petrology **50**, 1829-1855
[5] Belousova et al. (2002) Journal of Geochemical Exploration **76**, 45-49
[6] Jennings et al. (2011) Geology **39**, 863-866
[7] McLeod et al. (2011) Journal of Petrology **52**, 55-82
[8] Bruand et al. (2014) Journal of Petrology **(in press)**
[9] Gagnevin et al. (2010) Contributions to Mineralogy and Petrology **159**, 579-596
[10] Darling et al. (2009) Geology **37**, 927-930
[11] Fowler and Rollinson (2012) Geology **40**, 1079-1082

Isua Tourmaline – A Window to Boron Concentrations in the Eoarchean?

E. Grew[1], R. Dymek[2], J. De Hoog[3], S. Harley[3], R. Hazen[4] & M. Yates[1]

[1]School of Earth and Climate Sciences, University of Maine, Orono, Maine 04469 USA
[2]Earth and Planetary Sciences, Washington University, St. Louis, MO 63130, USA
[3]School of GeoSciences, University of Edinburgh, Edinburgh EH9 3JW, UK
[4]Geophysical Laboratory, Carnegie Institution of Science, Washington, D.C. 20015, USA

Rationale for the study

Steven Benner [1] proposed that boron played an essential role in the stabilization of critical prebiotic organic compounds in the "RNA World" beginning at 4 Ga. Benner's scenario assumes that B concentrations in oceans and crust were sufficiently high to play this role at 4 Ga. The objective of proposed research is to determine whether this assumption is realistic by estimating what B concentrations might have been in the Eoarchean Era (~4-3.6 Ga) by analysing boron isotopes in tourmaline from the 3.7-3.8 Ga Isua supracrustals (West Greenland). Chaussidon and his colleagues [2,3] have developed a model relating sea-water B isotope composition to the proportion of B extracted from the Earth's mantle into the oceans and crust and concluded that most B extraction occurred between 4.0 Ga and 1.5 Ga.

Scope and methodology
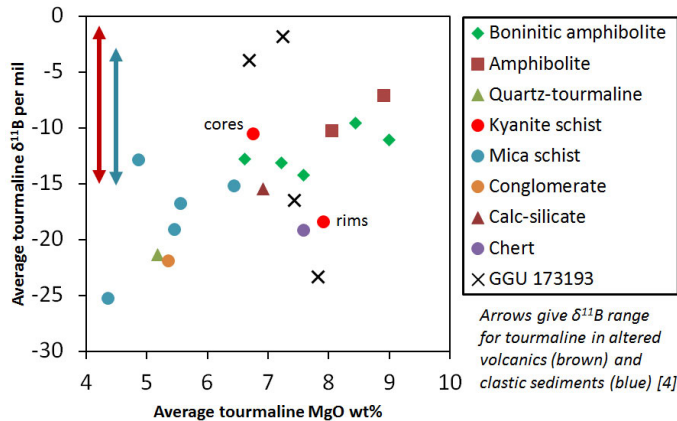
Figure 1. Summary of boron isotopic data from metasedimentary and metavolcanic rocks in the Isua Supracrustals

Eighteen samples of metasedimentary and metavolcanic rocks from the Isua Supracrustals were selected for in situ analysis of tourmaline with the Cameca 1270 ion microprobe from September 30 through October 11, 2013. From 2 to 8 grains of tourmaline were analysed in each of 17 samples (grains in the 18th sample were too close to the edge of the section to analyse), but many grains were analysed at two or more spots since most tourmaline grains are compositionally zoned. The data were calibrated using 3 tourmaline standards, which were run at the start of the day, several times during the day and at its close.

Results

In situ ion microprobe analyses of Isua tourmaline, which is schorl-dravite, gave average ($\pm$ 0.4 to 1.9‰) $\delta^{11}B$ = -7.1 to -14.2‰ (amphibolite), -12.9 to -25.3‰ (mica schist), -19.2‰ (metachert), -21.9‰ (metaconglomerate), where $\delta^{11}B$ = {[sample$^{11}B/^{10}B$ ، SRM 951$^{11}B/^{10}B$] $- 1$} $\times$ 1000)(Fig. 1). $\delta^{11}B$ varies from grain to grain in most samples, but in a few cases, tourmaline grains also show isotopic zoning, *e.g.*, large, euhedral crystals in the quartz tourmaline rock IS704-8, but trends from core to rim vary from one grain to another (Fig. 2). Isotopic zoning in tourmaline grains in kyanite schist IS629-7A (Fig 1) can be related to the breakdown of muscovite (Fig. 3). If muscovite had coexisted with the tourmaline cores, its breakdown would release boron with a lower $\delta^{11}B$ than the tourmaline cores since its B is in tetrahedral coordination, and tourmaline rims would have incorporated this lighter B, resulting in the observed zoning.
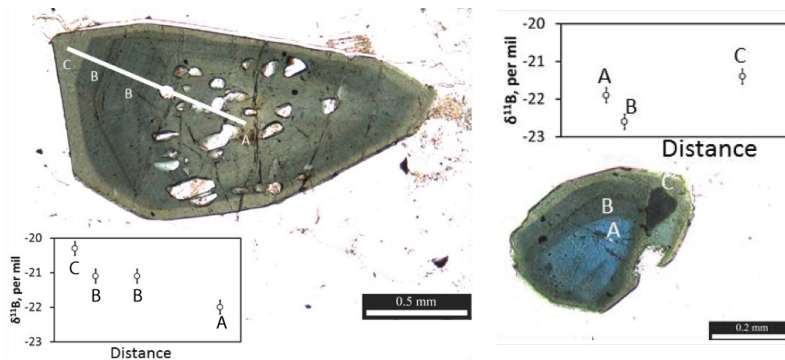
Figure 2. Boron isotopic composition of zoned tourmaline grains in IS704-8

rim $\delta^{11}B = -19.2 \pm 0.2$‰

core $\delta^{11}B = -10.6 \pm 0.2$‰

core $\delta^{11}B = -9.7 \pm 0.2$‰

rim $\delta^{11}B = -18.0 \pm 0.1$‰

Grain ~0.2 mm

Grain ~0.2 mm

Prism ~0.7 mm long

Ms

Bt

relict staurolite

Qz

Staurolite + chlorite + muscovite $\longrightarrow$ kyanite + biotite + H_2O.
Muscovite breakdown releases B with low $\delta^{11}B$ that is incorporated in tourmaline rims
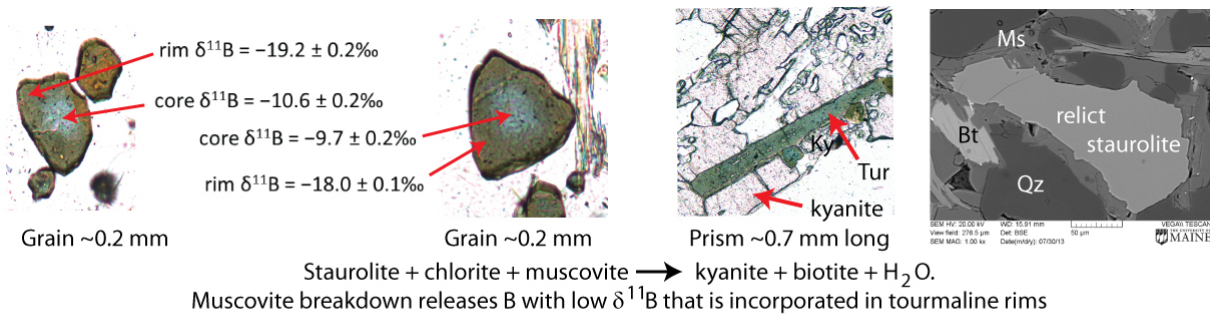
Figure 3. Kyanite schist IS629-7A: relating $\delta^{11}B$ zoning in tourmaline to muscovite breakdown

Tourmaline $\delta^{11}B$ values from Isua amphibolites having volcanic precursors overlap ranges of $\delta^{11}B$ values for tourmaline in younger altered volcanics rocks (Fig. 1). In contrast, $\delta^{11}B$ values from Isua schists and other rocks having sedimentary precursors are for the most part lighter (Fig. 1).

Implications

Boron in the schist samples could have been sourced in continental detritus as is the case for younger clastic sediments. However, rocks with 20-50 modal % tourmaline, e.g., the quartz-tourmaline rock (IS704-8) and association of tourmaline with chromite [$FeCr_2O_4$], chalcopyrite [$CuFeS_2$], gersdorffite [$(Ni,Co,Fe)AsS$], sphalerite (Fig. 4), galena [PbS], and pentlandite [$(Fe,Ni)_9S_8$] suggest a submarine exhalative origin, *i.e*., B, Zn, Cu, As and Pb were introduced hydrothermally into sedimentary and volcanic rocks prior to metamorphism together with Cr, Co and Ni remobilized from ultramafic rocks inserted in the Isua Supracrustals. Seawater was the primary source of these fluids. The tourmaline-bearing rocks are found in both the *ca*. 3700 Ma and *ca*. 3800 Ma terranes in the Isua belt. The highly negative $\delta^{11}B$ in the metamorphosed clastic sediments could have resulted from recycling of boron from older crustal rocks, *i.e*., the *ca*. 3800 Ma terrane and other terranes which are no longer exposed, and not from low seawater $\delta^{11}B$ [2,3]. Moreover, our findings suggest that boron might have been available to stabilize critical compounds in the "RNA World," although not necessarily in the form of borate in the desert environment envisaged by Benner [1].

Tur

$\delta^{11}B = -16.3$‰ (core),
-17.4 to -19.1‰ (rim)

sphalerite

Figure 4. Metamorphosed chert (173184): tourmaline associated with the zinc sulfide, sphalerite [ZnS]

References

[1] S.A. Benner et al. (2012) Accounts of Chemical Research **45**, 2025-2034
[2] M. Chaussidon and P.W.U. Appel (1997) Chemical Geology **136**, 171-180
[3] M. Chaussidon and F. Albarède (1992) Earth and Planetary Sciences Letters **108**, 229-241
[4] H.R. Marschall and S.Y. Jiang (2011) Elements **7**, 313-319
[5] E.S. Grew et al. (2013) Abstracts, American Geophysical Union Fall Meeting, in press

Constraints on Partial Resetting of Metamorphic White Micas by Combining *in situ* Isotopic Information with Geochronological (^{40}Ar/^{39}Ar) Data

R. Halama[1], M. Konrad-Schmolke[1], J.C.M. De Hoog[2], A. Schmidt[1] & M.Sudo[1]

[1]Institute of Earth and Environmental Science, University of Potsdam, D-14469 Potsdam, Germany
[2]School of GeoSciences, University of Edinburgh, Edinburgh EH9 3JW, UK

Scientific Report

Potassic white mica is ideally suited to exploit the recent advances in high spatial resolution analytical techniques because it is amenable to ^{40}Ar/^{39}Ar age dating, provides constraints on P-T conditions, and is an important carrier of fluid-mobile trace elements. The combination of *in situ* ^{40}Ar/^{39}Ar analyses with textural and geochemical data is often critical to understand the geological relevance of ^{40}Ar/^{39}Ar dates. In this study, we attempt to link effects of fluid-rock interaction to ^{40}Ar/^{39}Ar dates by using concentrations and isotopic compositions of boron (B) and lithium (Li) in phengites from partially overprinted metamorphic rocks from the Western Alpine Sesia-Lanzo Zone (SLZ) that contain phengites with compositional differences between cores and overprinted rims (Fig. 1).
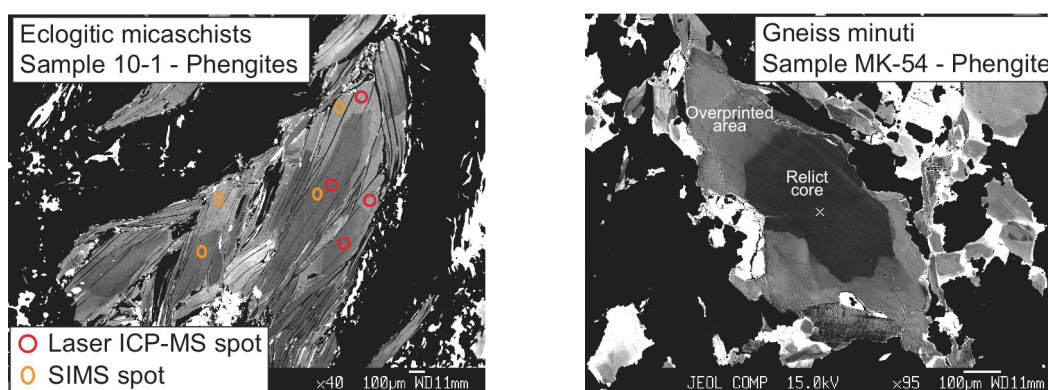
Fig. 1: Back-scattered electron (BSE) images of phengites in samples from the Sesia-Lanzo Zone. Relict cores are distinguished by relatively dark colours due to lower Fe contents compared to overprinted areas.

In the weakly deformed, eclogite-facies Eclogitic Micaschists (EMS) samples, Mg# and Na/(Na+K) in phengite decrease in overprinted areas due to changing phase assemblages and P-T-X_{H2O} conditions [1]. The variation in δ^{11}B among phengite cores (δ^{11}B = -21 to -10‰) shows lack of B isotopic equilibration on the km scale at peak metamorphic conditions (Fig. 2). During recrystallization of the overprinted areas, the fluid composition appears to be largely internally controlled by the rock because corresponding phengite cores and rims overlap in δ^7Li and δ^{11}B (-20 to -9‰) and the different samples preserve their differences in δ^{11}B (Fig. 2). Hence, no significant external fluid influx was required, and the decrease in B contents in the overprinted areas can be explained by internal redistribution during contemporaneous growth of paragonite (Fig. 2). Inverse isochrons were constructed from *in situ* ^{40}Ar/^{39}Ar data and they define two core crystallization periods of 88–82 and 77–74 Ma [2]. The younger cores have lower B contents than the older ones, suggesting that loss of B and resetting of the Ar isotopic system were related. Overprinted rims give younger apparent ^{40}Ar/^{39}Ar ages than the relict cores, suggesting that the metasomatic overprint during fluid-poor conditions caused resetting of the Ar isotope system, but had only minor effects on the B and Li isotope composition.

In greenschist-facies samples from the Gneiss Minuti (GM), relict cores and overprinted rims show major elemental differences, but B concentrations and δ^{11}B (-4 to -7 ‰) values overlap, demonstrating that B was not significantly leached from the overprinted parts (Fig. 2). In contrast to the EMS samples, δ^7Li increases together with Li contents in the overprinted areas, suggesting an external fluid influx. Relict phengite cores in the GM yield apparent ^{40}Ar/^{39}Ar ages between 58 and 67 Ma, which can be related to fluid flux in the adjacent Tallorno Shear Zone, dated at 65±3 Ma [2]. This interpretation is supported by the overlap in δ^{11}B values between cores of the GM unit and mylonitic

phengite from the TSZ. Overprinted phengite rims in the GM unit yield a continuous distribution of younger $^{40}Ar/^{39}Ar$ ages (58-33 Ma), indicating either continuous re-crystallization or the variable influence of a discrete greenschist-facies event that caused incomplete rejuvenation. The latter interpretation is supported by the changes in Li isotope composition in the rims (Fig. 2).

In summary, fluid-induced resetting of Ar isotopes in phengitic mica is controlled by deformation and associated fluid flux during exhumation and juxtaposition of two tectonometamorphic segments in the SLZ. Our study underlines the importance of metasomatic processes for interpretation of $^{40}Ar/^{39}Ar$ data in partially metasomatised rocks and shows that the combination of B-Li isotopic data with *in situ* geochronological data can provide valuable insights into the petrogenetic evolution of metamorphic rocks.
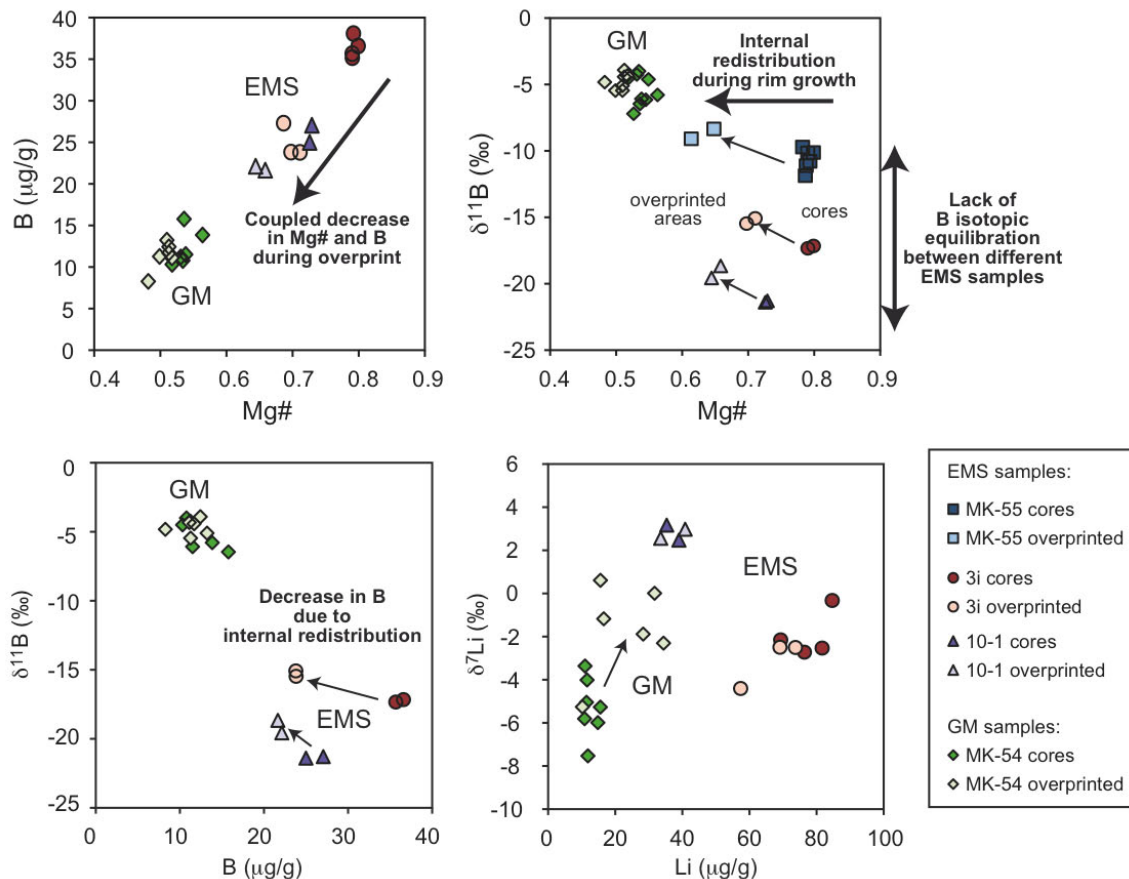
Fig. 2: Results of *in situ* geochemical and isotopic analyses of phengites from Sesia-Lanzo Zone samples.

References
[1] M. Konrad-Schmolke et al. (2011) Journal of Petrology **52**, 457-486
[2] R. Halama et al. (2014) Geochimica et Cosmochimica Acta **126**, 475-494

Tracking Pre-Eruptive Degassing at Laki, SE Iceland, through Trace Element Diffusion in Plagioclase

M.E. Hartley[1], J. Maclennan[1], M. Edmonds[1], D.J. Morgan[2] & T. Thordarson[3]

[1]Department of Earth Sciences, University of Cambridge, Cambridge CB2 3EQ, UK
[2]School of Earth and Environment, University of Leeds, Leeds LS2 9JT, UK
[3]School of GeoSciences, University of Edinburgh, Edinburgh EH9 3JW, UK

Introduction

Diffusion of minor and trace elements in magmatic crystals can provide important information on the timescales of magma ascent, mixing and degassing in the lead-up to large eruptions. The aim of this project was to use diffusion modelling in zoned phenocrysts to estimate timescales of CO_2 degassing prior to the AD 1783 Laki eruption, SE Iceland. Olivine-hosted melt inclusions from Laki range from volatile-rich (5000 ppm CO_2) to almost completely degassed (<50 ppm CO_2) [1]. These melt inclusions were trapped at pressures from <0.1 to >7 kbar, and the melt inclusions preserve a record of concurrent degassing and crystallisation. Using CO_2 and trace element data obtained by SIMS (IMF proposal 454/1011, 'Laki Revisited'), the total CO_2 mass release from the Laki magma is calculated to be on the order of 304 Mt [1]. By combining timescale constraints with model predictions of total CO_2 release from Laki [ref], we aim to estimate the mass flux of CO_2 to the surface in the premonitory phases of the Laki eruption. This will be of great importance for developing and refining forecasting models for giant Icelandic eruptions, in particular by investigating the applicability of gas flux monitoring in Iceland.

Approach

Zoned plagioclase macrocrysts from Laki often have high-anorthite (An_{84}-An_{89}) cores surrounded by oscillatory-zoned (An_{74}-An_{80}) mantles and labradoritic (An_{55}-An_{70}) rims. The plagioclase mantle and rim compositions can be reproduced by reverse fractional crystallisation of the Laki carrier melt, but the high-anorthite core compositions cannot be reproduced by fractional crystallisation modelling [2]. The plagioclase cores are therefore xenocrystic in origin, and were mixed into the Laki carrier liquid during the earliest stages of the evolution of the Laki magma. The growth of the plagioclase mantles thus represents one of the earliest magmatic processes in the history of the Laki magma, and it is likely that the growth of the first olivine crystals from the Laki magma occurred concurrently with the growth of the plagioclase mantles. The crystallisation of the plagioclase mantles is therefore expected to be concurrent with melt inclusion entrapment in the Laki olivines (Fig. 1). Diffusion of trace elements such as Mg and Sr across the 'core-mantle boundary' in the plagioclase macrocrysts (Fig. 1) is expected to provide a maximum timescale for processes occurring early in Laki's magmatic history, including melt inclusion entrapment. By combining timescale information with models of deep CO_2 degassing in the Laki magmatic system, we aim to reconstruct the expected CO_2 flux to the surface in the years preceding the Laki eruption.
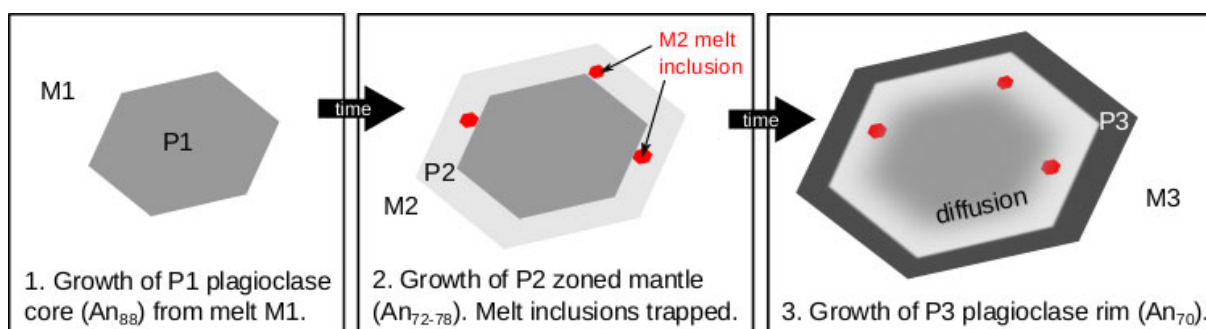
Fig. 1. Cartoon showing how evolving melt compositions can be recorded in crystal zonation and melt inclusions. In this simple model, the melt composition changes from M1 to M3 over time, and the composition of plagioclase crystallising from the melt changes from P1 to P3. Laki plagioclases have highly anorthitic P1 cores that cannot have crystallised from the Laki parental magma. The P1 crystals were mixed into the Laki parental melt M2. Melt inclusions with M2 compositions were trapped during the growth of P2 plagioclase mantles. Diffusive exchange between plagioclase zones P1 and P2 depends on the time between snapshots (2) and (3). This timescale, when combined with CO2 concentrations in the melt inclusions, provides a maximum timescale of deep CO_2 degassing from the Laki magma.

Results

We analysed selected trace and rare earth elements in rim-to-core profiles across sixteen plagioclase macrocrysts from Laki. Profiles consist of 6-15 point analyses with an average separation of 30 µm between points. Fig. 2 shows the variation in Mg and Sr contents across two profiles. Most of the Laki plagioclase macrocrysts show a positive correlation between Mg and Sr; however, some macrocrysts or zones within macrocrysts show a strong anticorrelation between Mg and Sr. Absolute elemental concentrations in the plagioclases are calculated by normalising ^{30}Si to the plagioclase SiO_2 content, determined by EPMA. To date we have only obtained EPMA data for around half of the crystals analysed by SIMS, so the data presented in Fig. 2 were calculated using an assumed SiO_2 content of 47 wt.% for the Laki plagioclases.
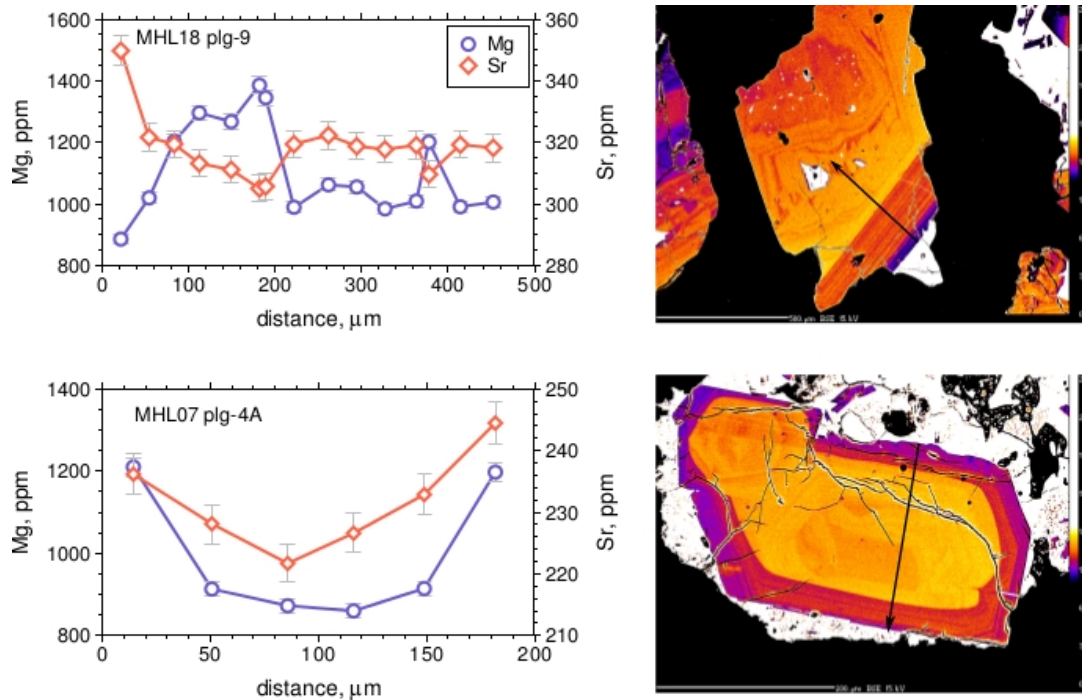
Fig. 2. Compositional profiles across two plagioclase macrocrysts from Laki. The profile locations are shown by the black arrows in the false-coloured SEM images of the crystals.

Further work

Analyses of Laki plagioclase profiles by EPMA needs to be completed before diffusion profiles can be fitted to the data, since Mg and Sr diffusion coefficients in plagioclase are dependent on the anorthite content of the plagioclase, e.g. [3]. This work is ongoing. Once the dataset is complete, we will fit 2-D diffusion models to the data in order to obtain direct estimates of timescales between crystal growth, melt inclusion entrapment and eruption. We will link timescale estimates to the evolution of the Laki magma body by integrating the diffusion modelling results with the record of cooling and crystallisation preserved in melt inclusions. We will use mineral-melt trace element partition coefficients to calculate the composition of plagioclase in equilibrium with the olivine-hosted melt inclusions, and thereby correlate the melt inclusion compositions with the growth of the plagioclase mantles. The trace element data will also be used to test the hypothesis that the high-anorthite cores of the Laki plagioclases crystalised from depleted melts of the shallow mantle [2]. Variability in trace element ratios such as La/Y and Sr/Y in the plagioclase macrocrysts is expected to reflect the diversity of primary melt compositions supplied to the lower crust beneath Laki.

References

[1] M.E. Hartley et al. (2014) Earth Planet. Sci. Lett., in press
[2] D.A. Neave et al. (2013) J. Petrol., **54**, 1661-1690
[3] K. Faak et al. (2013) Geochim. Cosmochim. Acta, **123**, 195-217

The Origin of Ferropicrite from Deep Melting of Recycled Material in the Convecting Mantle: A Melt Inclusion Study

E.S. Jennings[1], S.A. Gibson[1], J. Maclennan[1]

[1]Dept. Earth Sciences, University of Cambridge, Cambridge, UK. CB2 3EQ, UK

Background

Ferropicrite is a rare but important magma type, found exclusively in association with Continental Flood Basalts (CFBs), so is thought to be generated by melting in mantle plumes beneath thick lithosphere [1]. It is a primitive mantle melt with >12 wt % MgO and >~ 13 wt % FeO, with distinctive low Al_2O_3, and fractionated HREEs. Our study uses whole rock and olivine-hosted melt inclusion (MI) trace element geochemistry of ferropicrite to deduce the origin of its distinctive geochemical characteristics and to test the hypothesis that it is from low fraction, high pressure melting of mantle pyroxenite [1]. The presence of pyroxenite in the mantle has important implications for subduction recycling of oceanic lithopshere.

We initially obtained SIMS data of picrite MIs from the Parana-Etendeka Large Igneous Province (LIP) in 2012 (IMF460/0512). Picrite originates from plume melting of mantle peridotite, so forms a useful comparison when interpreting the ferropicrite data. Only a small number of ferropicrite MIs were analysed due to sample limitations. New ferropicrite samples from the Antarctic Karoo province [2,3] and a new sample from the Etendeka province were then obtained, and SIMS analyses of 65 ferropicrite MIs were carried out in November 2013. Here we report the preliminary results and data interpretation from this session (IMF482/0513).

Results

1) Melt inclusion homogeneity and relationship to whole rock chemistry

A surprising result of this study is that melt inclusion populations in ferropicrite samples, in particular the Antarctic samples, are extremely homogeneous, so each MI has a composition almost identical to the bulk rock (fig. 1a-c). This validates the use of whole rock geochemistry in approximating magma chemistry. The homogeneity is surprising as it is not observed in other studies; for example, highly heterogeneous MIs observed in some Icelandic samples have been explained by olivine crystallisation and inclusion trapping before instantaneous mantle melts are fully homogenised [4].
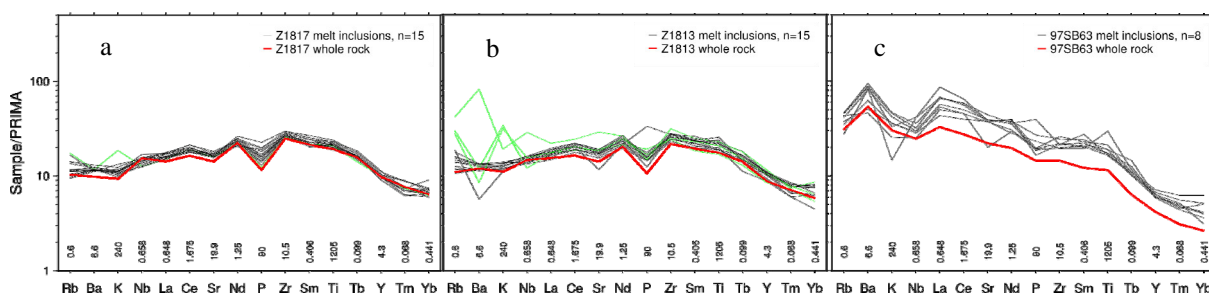
Figure 1 Multi-element plots showing trace element distribution in MIs and their respective host rock. a) Antarctic ferropicrite Z1817.3 b) Antarctic ferropicrite Z1813.1 c) Etendeka ferropicrite 97SB63. Green lines show those inclusions showing signs of secondary alteration and/or crustal contamination.

To explain the Antarctic samples, mantle melts must either have been initially homogeneous, or melts homogenised rapidly in magma chambers prior to olivine crystallisation. It is unlikely that ferropicrite melt was originally homogeneous, as pyroxenite-bearing mantle (probably in a veined configuration) is by definition heterogeneous. However, ferropicrite melt is high temperature and low viscosity (fig. 2). This favours onset of vigorous convection, eradicating initial melt heterogeneity. Unfortunately, this rules out discovering a more 'extreme' ferropicritic end-member composition in the MIs, derived from a higher proportion of pyroxenite-derived melt, which was part of the original rationale of the project.

2) Lithospheric contamination in MIs

Fig. 1 shows three of the seven analysed samples. Most MIs show no sign of contamination relative to the whole rock, except for a small subset (highlighted in green). These may show primary crustal assimilation, although the majority of contaminated inclusions have peaks only on fluid-mobile elements, which may instead be caused by secondary hydrous alteration of the inclusions. Understanding contamination in the whole rock trace element chemistry is difficult as trace element concentrations in the recycled component of the mantle source are poorly constrained, although on the basis of isotopic evidence, contamination levels may be low (<15%). This means that incompatible trace element concentrations, except for the most fluid-mobile elements, in both MIs and whole rock preserve their primary mantle signature, and so can be used for modelling the mantle source mineralogy of the ferropicrites.
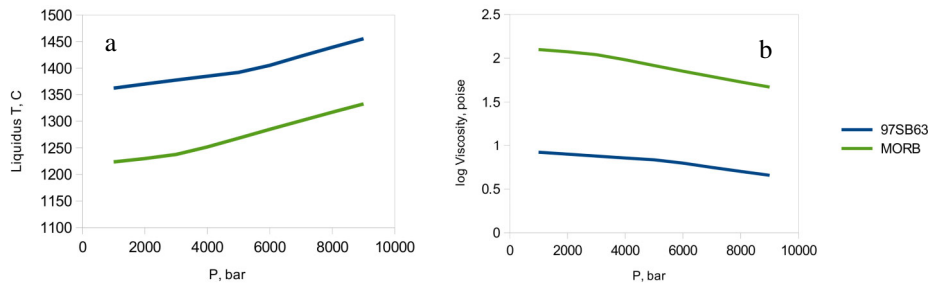
Figure 2 Viscosity, density and temperature of ferropicrite melt (blue). MORB is shown for comparison (green).

3) Mantle source of ferropicrite melt inclusions

Modelling the mantle source mineralogy of the Parana-Etendeka and Karoo ferropicrites is a work in progress. A pyroxenite mineral assemblage should a) melt deeper, b) have different bulk partition coefficients during melting and c) have a different melting reaction to peridotite. We can use these features to explore how a pyroxenite component in the source will affect the chemistry of the melts, and see if this can explain the distinctive trace element features in ferropicrite. Some results of preliminary models are shown in fig. 3; they indicate that, for a realistic melt fraction (F) of 0.2 the Etendeka picrites derive from a peridotite source with a minor contribution from pyroxenite. At F = 0.12 for the ferropicrites, a source modal mineralogy of 45% garnet and 55% cpx is required, which falls in the range of natural pyroxenites and eclogites.
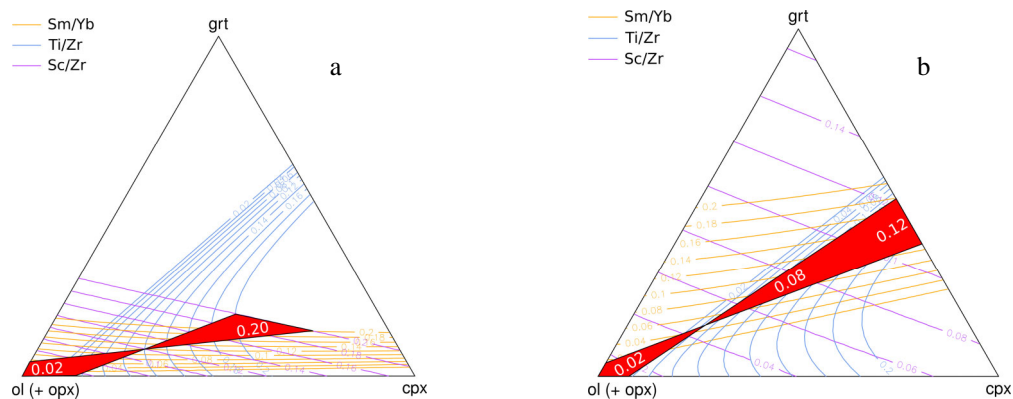
Figure 3 a) Picrite sample 97SB33 and b) Ferropicrite sample 97SB63. Contours represent the modal mineralogy required in the mantle source in order to reproduce the data for a given trace element ratio at given melt fractions (denoted by numbers on contours), using D values from [5]. a) uses a depleted mantle source, b) is enriched. Crossing contours denote a common solution; these regions are highlighted in red, where numbers in white indicate approximate melt fraction for the solution. To produce ferropicrite a lower proportion of olivine is required at a given F relative to picrite.

References

[1] Gibson (2002) Earth and Planetary Science Letters **195**, 59-74 [2] Heinonen and Luttinen (2008) Lithos **105**, 347-364 [3] Riley et al. (2005) Journal of Petrology **46**, 1489-1524 [4] Maclennan et al. (2003) Journal of Geophysical Research **108**, 2007 [5] Tuff et al. (2007) Journal of Petrology **46**, 2023-2058

Origin of Bimodal Chemical Signatures in Primitive Lesser Antilles Arc Olivines Investigated Using Oxygen Isotopes

H. Johnson[1], M. Thirlwall[1] & C. Manning[1]

[1]Department of Earth Sciences, Royal Holloway, University of London, Egham TW20 0EX, UK

Introduction

Olivine is the first fractionating phase from a mafic melt and as such can provide valuable insights into early petrogenetic processes and source compositions. Previous LA-ICP-MS analyses undertaken as part of this study on Lesser Antilles olivines identified chemical bimodalities in several elements. A group of lower calcium olivines (LCO) exhibit ranges in CaO contents between 0.02-0.11 wt% over a forsterite range of Fo_{80-91} compared to 0.12-0.28 wt% in the remaining olivines (Figure 1).
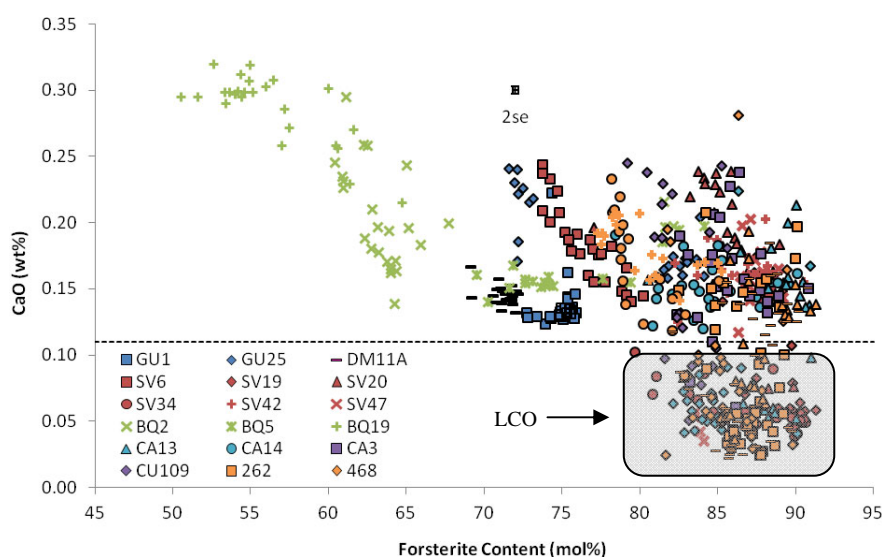
Figure 1. CaO concentrations with forsterite content. The dashed line shows a concentration of 0.11 wt% which has been used as an upper limit for defining the LCO (shown by the grey rectangle).

The LCO group also exhibit lower Cr, Y, Yb, Al_2O_3 and in some cases Sc than the remaining olivines at a given forsterite content; Zr/Y ratios are higher (up to 11). Mantle olivines in the literature share several characteristics with the LCO, such as low CaO and Cr contents, but exhibit higher forsterite contents ([1],[2]).

Reasoning for using $\delta^{18}O$

Oxygen is one of the few isotopic systems that can be successfully measured in olivines and should not be affected by fractional crystallisation. Therefore variations in $\delta^{18}O$ should highlight any isotopically distinct sources. Mantle olivine has been shown to have consistent $\delta^{18}O$ of 5.18 ±0.3‰ [3]. Consequently $\delta^{18}O$ can also be used to test the hypothesis that the LCO are mantle xenocrysts.

In addition a tentative negative correlation was observed between the abundance of LCO in the host lavas and whole rock $^{143}Nd/^{144}Nd$ ratios suggesting that the LCO may represent an elevated level of sediment in their parent melts. Sediment $\delta^{18}O$ is generally higher than that of parent melts suggesting that if the LCO are a result of increased sediment addition they may also have higher $\delta^{18}O$ than the higher CaO olivines.

Results

Olivines from 10 host lavas that have previously been analysed by LA-ICP-MS were analysed for $\delta^{18}O$. Both LCO and higher CaO olivines were targeted. There is an overall negative correlation between forsterite content and $\delta^{18}O$ of the analysed olivines. In general the olivines from the more northerly islands (Guadeloupe and Dominica) show higher $\delta^{18}O$ values than those from the south of the arc (St. Vincent, Carriacou and Grenada).

Mantle xenocrysts?

The LCO do not all show low enough $\delta^{18}O$ to meet the criteria set in [3] for mantle olivines (Figure 2). It would therefore appear unlikely that the LCO have crystallised from the mantle and erupted as xenocrysts.
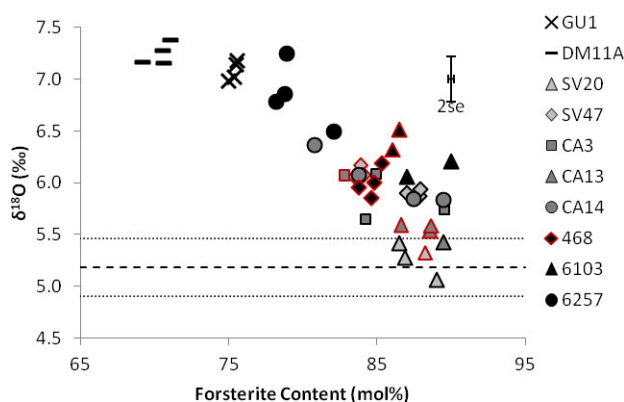
Figure 2. $\delta^{18}O$ contents in the analysed olivines showing only one LCO (outline in red) plotting in the mantle olivine [3] field (5.18‰ shown by dashed line with errors shown by dotted lines).

Isotopically different sources?

There is little isotopic difference between the LCO and the higher CaO olivines (Figure 3). This would suggest that if the two populations crystallised from different sources then these sources would have had similar oxygen isotope compositions.
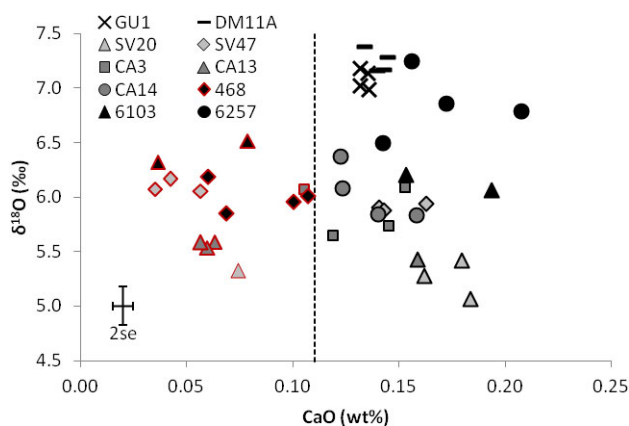
Figure 3. $\delta^{18}O$ contents in the LCO (outlined in red) compared to the higher CaO olivines showing no distinct isotopic differences. The dashed line shows 0.11 wt% CaO, the upper limit for the LCO.

Increased sediment input?

As seen in Figure 3, the LCO show comparable contents of $\delta^{18}O$ suggesting that if sediment input is higher in the parent melts of the LCO it is not visible in the oxygen isotope ratios.

Conclusions

$\delta^{18}O$ results show that the LCO are not mantle xenocrysts. They are likely to have crystallised from a different parent melt to that from which the higher CaO olivines crystallised but not from an isotopically (in terms of oxygen) different source. This would suggest differing processes occur within the magmatic plumbing system after melting of an isotopically similar source to produce the two populations.

References

[1] J.C.M. De Hoog et al. (2010) Chemical Geology **270**, 196-215
[2] N.J. Hirano et al. (2004) Contributions to Mineralogy and Petrology **148**, 47-54
[3] D. Mattey et al. (1994) Earth and Planetary Science Letters **128**, 231-241

The Influence of Subducting Components on Central Andean, Cenozoic Arc Magmas: Evidence from Boron Isotope Systematics

R. Jones[1], L. Kirstein[1], R. Hinton[1], S. Kasemann[2], & T. Elliott[3]

[1]School of GeoSciences, University of Edinburgh, Edinburgh, EH9 3JW, UK
[2] Department of Geosciences, University of Bremen, Germany
[3]Department of Earth Sciences, University of Bristol, BS8 1RJ, UK

Introduction

At convergent plate boundaries, such as the Andean margin, volatiles and crustal material are transported into the mantle by the subducting plate. The recycling of subducted material to mantle and crustal reservoirs, as well as the location and mode (slab-derived fluids versus silicate melts) of mass transfer from the subducting plate to arc magmas, remain outstanding issues in our understanding of subduction zones. The southern Central Andes provide a particularly interesting area to investigate these processes as the plate tectonic configuration of the Andean convergent margin has changed over the course of the Cenozoic. Specifically, the angle of the subducting Nazca plate has shallowed since the early Miocene (~18 Ma) [1]. This makes the southern Central Andes an ideal location for investigating how changing geodynamic settings may influence the chemistry of arc magmas, and in particular how the contribution and recycling of subducting components (altered oceanic crust (AOC), serpentinised oceanic mantle lithosphere, oceanic and continentally derived sediments) to arc magmas, may change over time with the angle of the subducting slab.

Boron (B) concentrations and isotope ratios have been identified as sensitive indicators of subducting slab components in arc magmas. This is because (1) B is highly fluid mobile during slab dehydration [2]; (2) B behaves incompatibly in magmatic processes [3]; (3) B is relatively enriched in components of the subducting slab compared to the mantle (Fig. 1) [e.g., 4, 5-7]; and (4) these different components/reservoirs have distinct B isotope compositions (Fig. 1). The higher B concentrations found in arc magmatic rocks compared to those found in intra-plate settings, together with the correlation between B and [10]Be (a cosmogenic radionuclide which can only be produced in the upper atmosphere and is strongly enriched in sediments) enrichment, has been used to support boron addition to arc magmas from subducting components [e.g., 2, 8, 9].
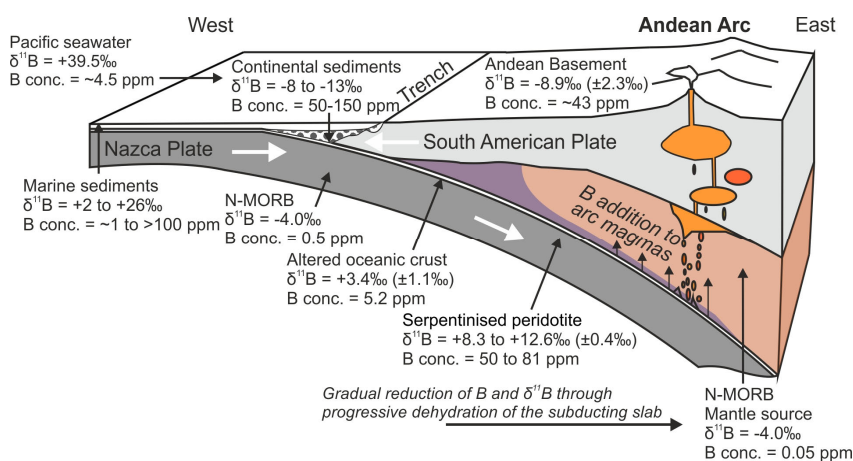
Figure 1. Boron concentrations and isotope ratios of different boron reservoirs present along the Andean convergent margin [4-7, 10, 11].

In order to investigate the recycling of subducted material to southern Central Andean (~29.5 and 31 °S) arc magmas, we analysed boron isotope and select trace element compositions of pyroxene and zircon hosted melt inclusions by secondary ion mass spectrometry (SIMS). The melt inclusions were obtained from eight samples of Cenozoic arc magmatic rocks ranging in composition from basaltic andesites to dacites. Melt inclusions were analysed as they are protected by the surrounding host phenocryst phase from late stage processes occurring in the melt and post depositional alteration [12].

Results

Boron concentrations obtained from pyroxene and zircon hosted melt inclusions range from 9 to 218 ppm and $\delta^{11}B$ values range from -5.4 ±1.6 ‰ to +8.6 ±1.2 ‰ (Fig. 2) (uncertainties/error bars given on individual $\delta^{11}B$ values are propagated analytical uncertainties quoted at the 2σ level).

The most significant feature of the data is the differences in $\delta^{11}B$ values and B/Nb ratios obtained for samples of different ages (Paleocene, Oligocene and Miocene). Boron isotope values obtained for the Paleocene sample (RJ1111 (61.2 ±1.0 Ma)) are positive and range between +0.7 ±0.9 ‰ and +3.7 ±1.2 ‰. These are accompanied by relatively high B/Nb ratios of between 15.6 and 20.7. The Oligocene samples (MQ153 (25.2 ±0.3 Ma), ZN122 (24.8 ±0.4 Ma) and Z27 (23.2 ±0.3 Ma)) produced generally negative $\delta^{11}B$ values between -5.4 ±1.6 ‰ and +0.9 ±1.7 ‰ and low, tightly grouped B/Nb ratios of between 1.5 and 5.7. Boron isotope values obtained for melt inclusions present in the Miocene samples (AM0887 (19.3 ±0.3 Ma), 1026 (18.2 ±0.3 Ma) and RF65/RF62 (17.1 ±0.6 Ma)) are positive and range between +1.5 ±1.2 ‰ and +8.6 ±1.2 ‰, with B/Nb ratios ranging between 4.4 and 36.3.
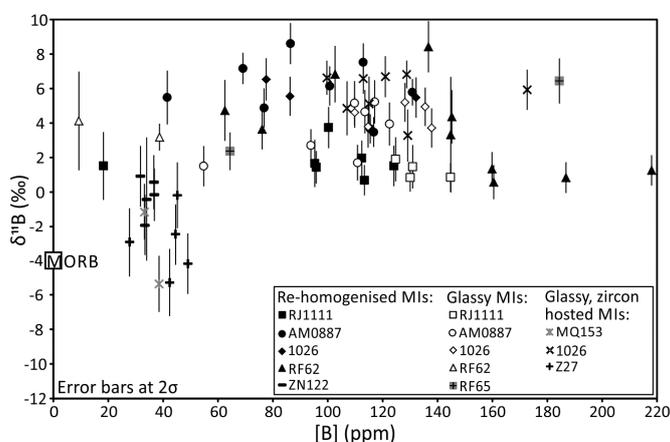
Figure 2. Boron concentrations (ppm) plotted against $\delta^{11}B$ (‰) for pyroxene (filled symbols represent re-homogenised melt inclusions) and zircon hosted melt inclusions (MIs).

Interpretations

Multi-component mixing models have been generated suggesting the primary source of the boron present in Paleocene and Oligocene arc magmas is fluid derived from AOC on the subducting oceanic plate, with a minor component derived from dehydrating serpentinite. The lower $\delta^{11}B$ values and B/Nb ratios obtained for the Oligocene arc magmatic rocks suggests a diminished influence of slab-derived fluids on the source of arc magmas, which is indicative of a great depth to the slab-mantle interface. The higher $\delta^{11}B$ values and B/Nb ratios obtained for the Miocene arc magmatic rocks has been interpreted as representing a greater influence of fluids derived from serpentinite dehydration on the source of the arc magmas. This is coeval with the subduction of a volcanic seamount chain (the Juan Férnandez Ridge) which has been associated with hydrated and serpentinited oceanic lithosphere [13]. Crustal assimilation of the Paleozoic – Mesozoic Andean basement, as the arc magmas migrate to the surface, is suggested to account for some of the intra-sample variation in $\delta^{11}B$ values and trace element signatures.

[1] G.A. Yañez, C.R. Ranero, R. von Huene, J. Díaz, Journal of Geophysical Research 106(2001) 6325 - 6345. [2] W.P. Leeman, V.B. Sisson, Reviews in Mineralogy and Geochemistry 33(1996) 645 - 707. [3] J.M. Brenan, E. Neroda, C.C. Lundstrom, H.F. Shaw, F.J. Ryerson, D.L. Phinney, Geochimica et Cosmochimica Acta 62(1998) 2129 - 2141. [4] M. Chaussidon, B. Marty, Science 269(1995) 383 - 386. [5] T. Ishikawa, E. Nakamura, Earth and Planetary Science Letters 117(1993) 567 - 580. [6] H.J. Smith, A.J. Spivack, H. Staudigel, S.R. Hart, Chemical Geology 126(1995) 119 - 135. [7] A.J. Spivack, J.M. Edmond, Geochimica et Cosmochimica Acta 51(1987) 1033 - 1043. [8] J.D. Morris, W.P. Leeman, F. Tera, Nature 344(1990) 31 - 36. [9] J.G. Ryan, J.D. Morris, F. Tera, W.P. Leeman, A. Tsuetkov, Science 270(1995) 625 - 627. [10] M. Chaussidon, A. Jambon, Earth and Planetary Science Letters 121(1994) 277-291. [11] S. Kasemann, J. Erzinger, G. Franz, Contributions to Mineralogy and Petrology 140(2000) 328 - 343. [12] A.V. Sobolev, Petrology 4(1996) 209 - 220. [13] H. Kopp, E.R. Flueh, C. Papenberg, D. Klaeschen, Tectonics 23(2004).

Ground-Truthing Cretaceous Nannofossil Productivity Proxies Using Single-Specimen Sr/Ca Data

J.A. Lees[1], C. Linnert[1], P.R. Bown[1], T. Dunkley Jones[2], S. Robinson[3] & J.R. Young[1]

[1]Dept of Earth Sciences, University College London, Gower Street, London WC1E 6BT
[2]School of Geog., Earth & Environmental Sciences, University of Birmingham, Edgbaston, Birmingham B15 2TT
[3]Dept of Earth Sciences, University of Oxford, South Parks Road, Oxford OX1 3AN

Reasons for investigation

In modern coccolithophores, coccolith-calcite Sr/Ca ratios positively correlate with both calcification and cellular growth rates [1, 2]. Opportunities for ground-truthing Cretaceous calcareous nannoplankton assemblage-based productivity proxies are limited. There are very few extant analogues for Cretaceous palaeofloristic environmental proxies, and very few sections have sufficiently well-preserved nannofossil records to provide meaningful quantitative data in tandem with a robust, independent geochemical proxy record. Sediments from a corehole in Mississippi (USA) provided just such an opportunity and are lithologically well disposed for the fine-fraction filtering technique required for separation of nannofossil taxa for SIMS analysis. This has allowed us to test for a fundamental link between changes in nannofossil productivity (as determined by Sr/Ca) and a $c.7°C$ surface-water cooling (from our novel TEX_{86} temperature record [3]), with its likely concomitant increased surface-water mixing and nutrient cycling.

Results

In total, 497 measurements of Sr/Ca, Mg/Ca and Al/Ca were made on 33 Late Cretaceous species from split microfractions of six Campanian to Maastrichtian samples that represent an estimated sea-surface temperature (SST) range of 28 to 36°C. We also measured the total organic carbon (TOC), which ranges from 0.27 to 1.02% in our measured samples. On Figures 1c, 2c and 3c, the higher TOC values (~1%) lie to the right, and the lower values (~0.3%) to the left. Below, we report only on the Sr/Ca, as the Mg/Ca and Al/Ca are variable and likely relate more to contaminant clay. To answer our original objectives (please note, these are very preliminary observations):

1. *Are interpretations of Cretaceous productivity taxa supported by Sr/Ca measurements on individual specimens? Biscutum ellipticum* (Figure 1) is the most-quoted 'high-productivity' species, with increased abundances being related predominantly to Cretaceous oceanic anoxic events, whilst *Watznaueria barnesiae* (Figure 2) is a purportedly 'low-productivity' species. Sr/Ca values are generally higher for *B. ellipticum* than for *W. barnesiae* (compare Figures 1c, 2c). Our count data show a distinct abundance decline in *B. ellipticum* (vs the mean) as SSTs and TOC decrease, with much lower abundances associated with the lowest SSTs/TOC. However, there is, intriguingly, an increase in mean Sr/Ca associated with the lowest SST and low TOC (Figure 1c). In our count data, *W. barnesiae* has highly variable abundance (vs the mean) associated with warmer SSTs, becoming more abundant with lowered SSTs and lower TOC, but markedly less abundant with much lower SSTs and low TOC. Its Sr/Ca values are, however, relatively stable, except for the sample at ~30°C, where values become widespread; we currently have no explanation for this.

2. *Do Cretaceous high- and low-productivity proxy taxa have similar offsets in Sr/Ca values to Cenozoic productivity proxies, such as* Coccolithus *and* Discoaster*?* We are evaluating this in collaboration with the separate TDJ study (Eocene-Oligocene) and a previous study by JAL, PRB and JRY (Paleocene-Eocene). What we *can* say is that there is distinct interspecies variability in the Cretaceous taxa (compare Figures 1c-3c).

3. *Do fossil heterococcoliths have different Sr/Ca values to holococcoliths and nannoliths, and so is calcification different between the three types of nannofossil?* Our hetero-/holococcolith and nannolith data show distinctive Sr/Ca ranges, but all plot within a range of heterococcolith values, suggesting somewhat similar calcification. For example, values for *Micula* (nannolith, Figure 3) are relatively low, but plot within the range for *Watznaueria* (heterococcolith, Figure 2). *Lucianorhabdus* (holococcolith, not figured) plots higher, around 2 to 3.5 mmol/mol Sr/Ca, but within the higher range of *Watznaueria*.

1a

1b *B. ellipticum (sample770-3-s33)*

1c Sr/Ca vs. palaeo SST: *Biscutum/Sollasites*

2a

2b *W. barnesiae (sample SHUQ615-5-s26)*

2c Sr/Ca vs. palaeo SST: *Watznaueria*

3a

3b *M. staurophora (sample490-5-6)*

3c Sr/Ca vs. palaeo SST: *Micula*
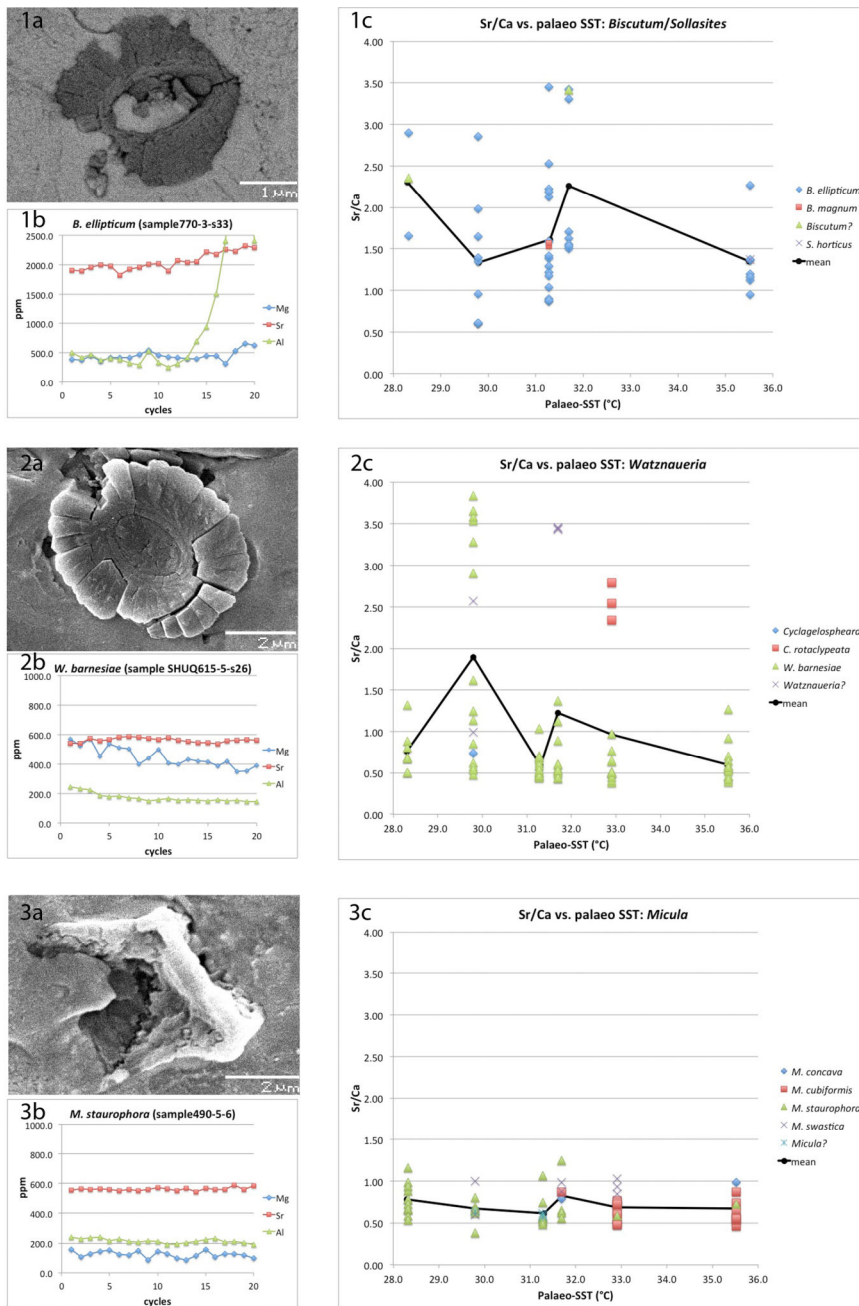
Future work

This is the first nannofossil-Sr/Ca data for the Mesozoic, adding to a growing collection of single-coccolith data generated by our working group from the Late Cretaceous through extant. From these, nannofossil-Sr/Ca appears to be viable to develop as an independent test of palaeoecological proxies, but to better understand data variability, we need a statistically-robust dataset and to focus on getting more data from fewer species (or getting more time on the SIMS). We intend to further our efforts to be world-leaders in nannofossil geochemical techniques that we have been at the forefront of developing.

References

[1] R.E.M. Rickaby et al. (2002) Global Biogeochemical Cycles **16**, 1006, doi:10.1029/2001GB001408
[2] H.M. Stoll et al. (2007) Deep-Sea Research II **54**, 581-600
[3] C. Linnert et al. (in review) Nature Communications

Changing Magma Storage Conditions during the Highly Calcic Pollara Eruptions of Salina (Italy)

H. Moretti[1], J. Gottsmann[1], J. Blundy[1] & R. Sulpizio[2]

[1]School of Earth Sciences, University of Bristol, Wills Memorial Building, Bristol BS8 1RJ, UK
[2]Universitá degli studi di Bari Aldo Moro, 70121, Bari, ITALY

Background

The island of Salina lies within the Aeolian archipelago at the intersection of an arcuate chain of volcanic seamounts and islands that form the volcanic front of the Ionian Subduction zone and a NNW-SSE trending chain of large volcanic islands that follow the course of the Tindari-Letojanni dextral strike-slip fault [1, 2]. The initial basaltic eruptions at Capo and Rivi date back to 244ka [1], followed by the felsic to mafic Fossa delle Felci eruptions (127-141ka), Porri (67-73ka) and the Pollara sequence (30-13ka). The Pollara sequence began with the extrusion of a dacitic lava at 30ka (Punta di Perciato), followed by a stable-column explosive lower Pollara (LPP) at 26.7ka and the unstable-column explosive concluding Upper Pollara (UPP) at 15.6ka [1].
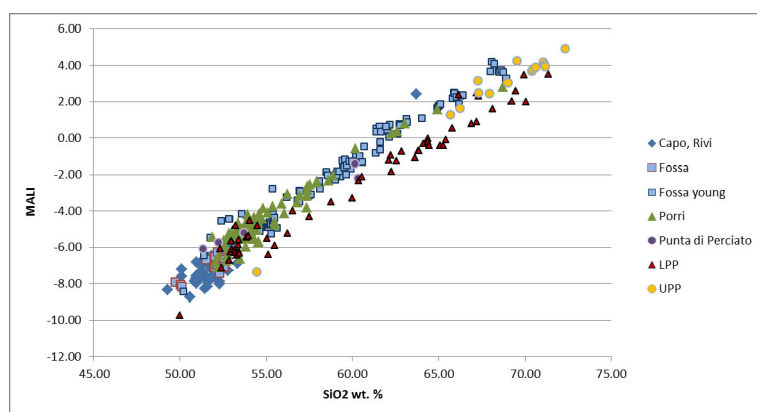
Fig 1: The modified alkali-lime index (MALI) [3] shows the evolved LPP eruption products (red triangles) to have a greater degree of calcium saturation.

Investigations across arc [2] show Salina to have the least overprinted fluid-subduction trace element pattern as evidenced by Ba/La ratios whereas peripheral islands in the arc have increasing geochemical evidence of inflow from the asthenosphere [1, 2]. Salina sequences have been described as mid to low-K calc-alkaline [1, 2] though *sensu strictu* they are calcic using the Peacock classification [4] and during the LPP became increasingly so (fig 1) with a flat iron enrichment trend that suggests magnetite fractionation in a strongly oxidising environment. This is at odds with the rest of the island's eruptions that have shown increasing crustal assimilation of an aluminous basement [1].

The Aeolian Islands have been modelled for depth of magma storage areas by Frezzotti et al. [1, 5] used quartz hosted CO_2 and $CO_2 + N_2 + H_2O$ fluid inclusions the Porri eruption to generalise for Salina, finding that initial melts evolve in the continental crust at 0.32 GPa (13km) and rise as short-lived shallow bodies at 0.12 GPa (4 km). The Pollara sequences are different, no quartz xenoliths survive which may suggest longer, shallow residence times and major element and trace element ratios all point to prolonged exposure to a calcium carbonate source (this study).

Evidence of a limestone basement

Samples collected from the LPP sequence in September 2012 included skarn-xenoliths and diopside-rich magmatic cumulates that suggest interaction between these recent eruptions and a possibly localised limestone basement (fig 2). Diopside phenocrysts from the later UPP have distinct oscillatory zoning that may result from disequilibrium reactions with the calcium carbonate and sub-micron diffusion profiles will be undertaken at Bristol to investigate this. The objective for the ion probe was to constrain the magmatic storage depths of the Pollara eruptions and any carbonate interaction zone.
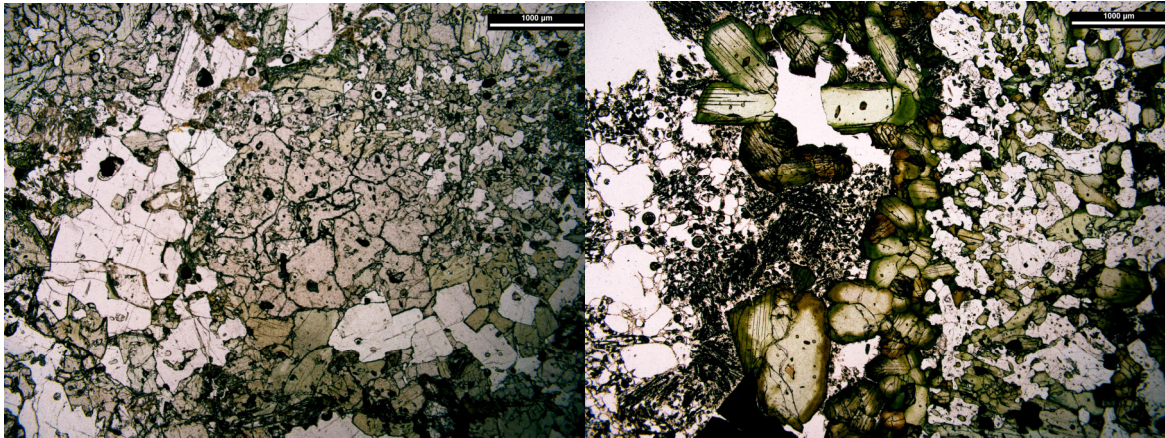
Fig 2: Photomicrographs of (left) skarn-cumulate from the LPP sequence containing Grossular Garnet, Anorthite, Diopside and magnetite; melt inclusions within a diopside magmatic cumulate (right) of the LPP.

Melt inclusions within the Pollara sequence

An initial visit to Edinburgh to use the Cameca 4f ion probe in week commencing November 11, 2013 allowed analysis of water, carbon (for CO_2) and trace element data for 40 melt inclusions. These were predominantly found in the skarn and magmatic cumulates and the uncalibrated values are plotted below (fig 3) which describes a water-rich (4.5 – 6 wt. %) magmatic cumulate body and a dry (0.01-0.3 wt. % H_2O) CO_2-rich skarn. A smaller number of melt inclusions were found in the scoria and pumice; mostly plotting between the two trends described by the cumulate plots and could suggest a degree of interaction between the proposed limestone basement and resident melt. Further samples are being mounted for the felsic LPP and UPP and these initial results are being calibrated using silica, magnesium and potassium values from the Bristol electron microprobe during week ending 28 February 2014 allowing corrected carbon values to be plotted and magma ascent paths to be calculated.
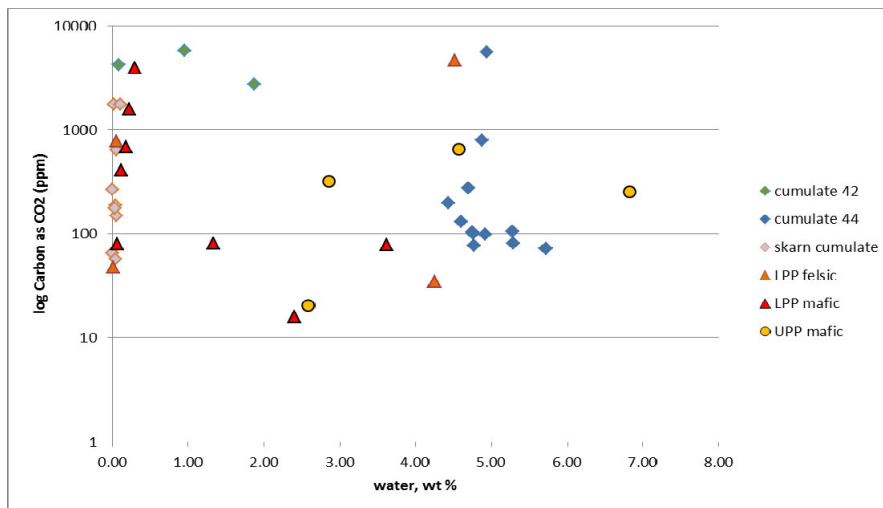
Fig 3: Plot of CO_2 (ppm) versus H_2O from melt inclusion analyses on the Cameca 4f ion probe at Edinburgh. A summary of the uncalibrated results are sent separately as an appendix.

References
[1] F. Lucchi et al. (2013) Geological Society Memoir **37**, 155-212
[2] L. Francalanci et al. (2007) in Beccaluva et al., Cenozoic volcanism in the Mediterranean area **418**, 235-264.
[3] B.R. Frost and C.D. Frost (2008), Journal of Petrology **49(1),** 1955-1969
[4] M.A. Peacock (1931) Journal of Geology, **39,** 54-67.
[5] M.L. Frezzotti et al. (2003) in De Vivo and Bodnar, Melt Inclusions in Volcanic Systems, 185-206.

Experimental Study of Magmas in the Altiplano-Puna Magma Body

D. Muir[1], J. Blundy[1], A. Rust[1] & R. Brooker[1]

[1] School of Earth Sciences, University of Bristol, Wills Memorial Building, Queens Road, Bristol, BS8 1RJ, UK

Introduction

The Altiplano-Puna magma body [1] (APMB; Fig. 1) in the central Andes is recognised as the largest known active magma body on Earth but little is known about the composition of magmas stored within this vast reservoir. The APMB is the likely source of magmas erupted in the Altiplano-Puna region of the central Andes. Erupted products in this region are exclusively silicic but dacites and rhyolites commonly contain magmatic enclaves of basaltic-andesite to andesite composition. These less evolved magmas are our best estimate of APMB magma compositions.

To test whether dacite melts can be produced from a basaltic-andesite bulk compositions at APMB conditions at equilibrium, we conducted piston cylinder experiments. Run conditions varied between 890 and 980°C and 0.5 and 1.1 GPa using the least evolved basaltic-andesite composition from a magmatic enclave from Uturuncu volcano, SW Bolivia as a starting material. Experiments were run under H_2O-saturated and -undersaturated conditions and were buffered at a fO_2 around Nickel-Nickel Oxide. Our aim was to determine whether basaltic-andesite magmas stored at equilibrium have dacite melts equivalent tow whole-rock compositions of erupted magmas at Uturuncu. If so, we could envisage a scenario where dacite melts buoyantly rise from the APMB to shallow pre-eruptive storage regions where they crystallise prior to eruption. In addition, our H_2O-saturated experiments provided an opportunity to investigate volatile solubility in silicic melts at APMB conditions.
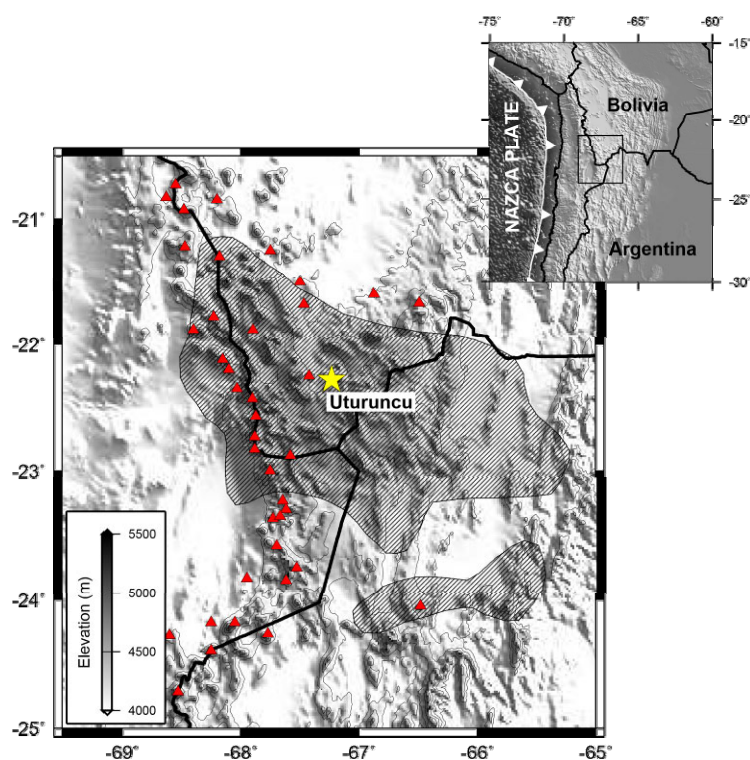
Figure 1. The extent of the APMB (cross-hatched area) which is thought to occur at depths >17 km (c. 0.6 GPa) below surface. Active volcanoes are shown by triangles. The inset map shows the location of the APMB in the Central Andes

Major and trace element concentrations of experimental glasses

Major and trace element concentrations were analysed in experimental glasses. Major and trace element compositions of equilibrium melts (glasses) at APMB conditions do not match erupted lava

whole-rock compositions from Utruruncu. Melts in H_2O-saturated experiments approximated dacite whole-rock compositions most closely but even in the lowest temperature runs with highest crystal fractions, K_2O, TiO_2 and FeO and Th could not be enriched sufficiently in the melt phase to match erupted whole-rock compositions. From isotopic studies we know that intermediate magmas erupted at Uturuncu have been subject to extensive crustal contamination. Potentially the differences between melt and natural lava major and trace element compositions could be accounted for by the addition of crustal melt, either in the APMB, or as magmas ascend and stagnate in shallower storage regions *en-route* to the surface.

Dissolved volatile contents in experimental melts

H_2O and CO_2 contents of volatile-saturated dacitic experimental glasses were analysed by SIMS. Dissolved H_2O contents remain relatively constant irrespective of pressure but CO_2 increases dramatically as pressure goes up (Fig. 2). Dissolved volatile contents in most experiments at 0.5 GPa and 0.8 GPa are similar to predictions from solubility models (Fig. 2). However, at 0.8 GPa at 980°C and in all runs at 1.1 GPa, dissolved volatile contents are much higher than expected; in 1.1 GPa experiments CO_2 is three times higher than predicted. As CO_2 was not added intentionally to capsules prior to running experiments the graphite furnace is the most likely source of the carbon which must diffuse into the capsule during the experiment. We anticipate the observed dissolved volatile enrichment from existing model predictions is most likely a quench effect where crystallisation reduces the melt volume effectively increasing the concentration of dissolved volatiles.
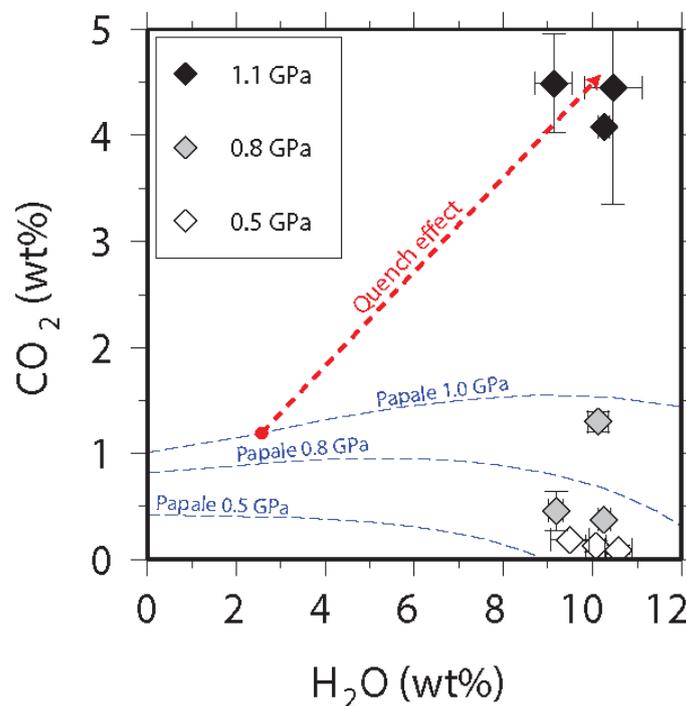
Figure 2. Dissolved H_2O and CO_2 concentrations of volatile-saturated experiment melts compared to existing volatile solubility models [2] at 950°C. The dashed red arrow demonstrates the quench enrichment required to increase CO_2 and H_2O in 1.1 GPa melts by a factor of 3.75 from 1.2 wt% and 2.7 wt% respectively.

References

[1] J. Chmielowski et al. (1999) Geophysical Research Letters **26**, 783-786
[2] P. Papale et al. (2006) Chemical Geology **229**, 78-95

Skuggafjöll: A Window into Deep Crystallisation, Degassing and Mixing in the Eastern Volcanic Zone of Iceland

D.A. Neave[1], J. Maclennan[1], M. Edmonds[1] & T. Thordarson[2]

[1]Department of Earth Sciences, University of Cambridge, Cambridge, CB2 3EQ, UK
[2]School of GeoSciences, University of Edinburgh, Edinburgh EH9 3JW, UK

Objectives

Recent studies have provided new insights into the nature of mixing and crystallisation processes in the plumbing systems of large basaltic fissure eruptions in the Eastern Volcanic Zone (EVZ) of Iceland. However, the effect of mixing on the CO_2 content of primitive basalts remains poorly understood. A number of studies have used Nb as a proxy for undegassed CO_2 and by knowing a CO_2/Nb for primitive melts it is possible to track how CO_2 degasses during magmatic evolution[2]. The environmentally impacting AD 1783 Laki eruption, which has been the focus of recent research, is comparatively evolved in composition (Mg# = 42) and as a consequence the earliest phases of magmatic evolution may have been overprinted. For example, olivine-hosted melt inclusions have low CO_2/Nb ratios (<<300) that are consistent with the melt having degassed much of its CO_2 by the time of melt inclusions entrapment.

This project uses pillow basalt samples from the Skuggafjöll table mountain, which are amongst the most primitive basalts in the EVZ (Mg# = 54), in order to constrain magmatic evolution and degassing processes in primitive melts from the EVZ. Project objectives include: (1) What was the primary CO_2 of the melt and the CO_2 flux into the system? (2) What was the extent of CO_2 degassing prior to eruption and how is degassing related to other magmatic processes such as crystallisation? (3) At what depth did these degassing and crystallisation processes take place? (4) What effect does magma mixing have on the CO_2 content of melts and melt inclusions?

Approach

A total of 110 olivine-hosted melt inclusions were analysed for major, trace and volatile elements. Olivines containing large, naturally quenched melt inclusions were picked from glassy pillow margins to minimise the effects of post-entrapment processes (**Figure 1**). Inclusions and glasses were analysed for CO_2, H_2O, F and selected trace elements (REEs, Nb and Zr) using a Cameca IMS-4f ion microprobe at the University of Edinburgh. Major elements, Cl and S were measured using a Cameca SX-100 electron microprobe at the University of Cambridge.
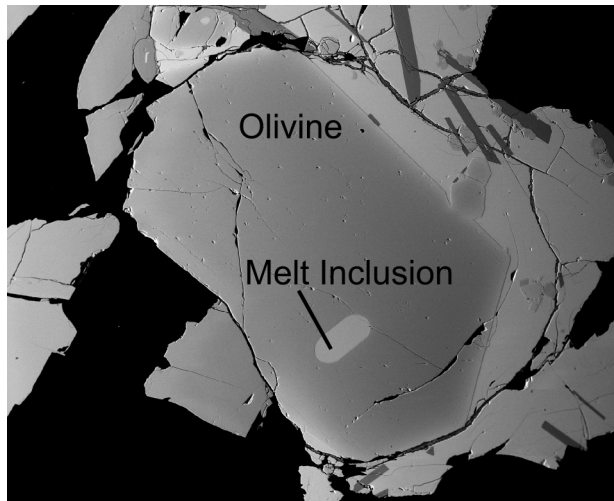
Figure 1. Backscattered scanning electron (BSE-SEM) image of an olivine macrocryst from Skuggafjöll showing a typical, glassy melt inclusion (>100 μm).

Results

Most olivine grains have tightly constrained forsterite contents of Fo_{85-87}, indicating that they are primitive and suitable for investigating magmatic processes recorded in primitive EVZ melts.

The major element compositions of melt inclusions indicate that post-entrapment crystallisation has been minimal (<5%). Trace element variability in melt inclusions is greater than analytical error for elements which can be determined with high precision such as Zr & Ce (**Figure 2**). Strong correlations are observed between incompatible trace element concentrations (e.g. Zr, Nb, La, Ce) and between trace element ratios (e.g. Ce/Y). Matrix glasses are significantly enriched in trace elements with respect to the melt inclusions and are compositionally homogeneous.
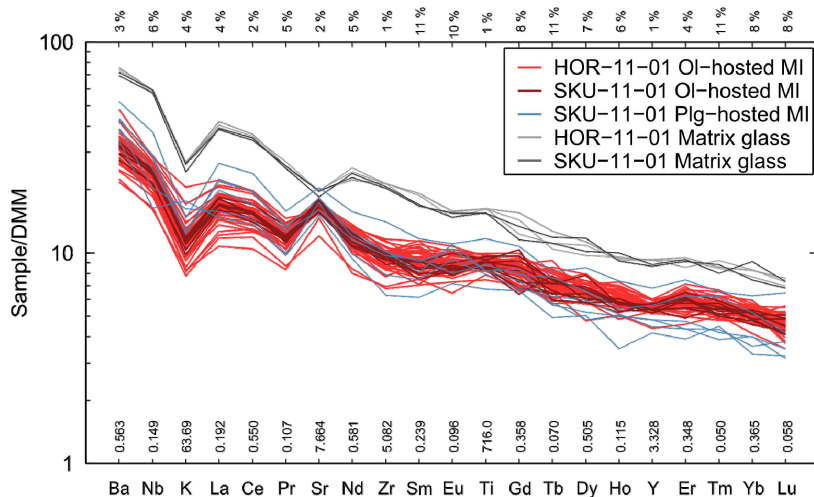
Figure 2 Depleted MORB Mantle (DMM) normalised trace element spider diagram of Skuggafjöll melt inclusions and matrix glasses. 1σ % relative errors are shown along the top and normalisation values along the bottom.

Both melt inclusions and matrix glasses contain ~0.38 wt.% H_2O (**Figure 3**). This relatively high H_2O content is consistent with rapid diffusive re-equilibration of melt inclusion H_2O with their carrier melt immediately before rapid quenching in a subglacial eruption during the last glacial period (>10 ka). In contrast, the CO_2 concentration of melt inclusions is variable and ranges from 200 to up to 1200 ppm (**Figure 3**). CO_2/Nb values reach up to 410, consistent with the only other study of volatiles and trace elements in Iceland (**Figure 4**)[1]. High CO_2/Nb values suggest that some melt inclusions preserve melts that have experienced minimal degassing prior to entrapment, giving an estimate of the CO_2 content of primary Icelandic melts.

The negative correlation between the CO_2 and trace element content of melt inclusions from Skuggafjöll (**Figure 4**) contrasts with positive correlations in datasets of CO_2 undegassed melt inclusions[2]. This anti-correlation could be interpreted as a record of concurrent crystallisation and degassing. However negative correlations are also observed between CO_2 and trace element ratios such as Ce/Y (**Figure 4**). The most depleted, low Ce/Y inclusions have the highest CO_2 and the most enriched, high Ce/Y inclusions the lowest. This is the first time that such an observation has been made, and suggests that CO_2 behaved differently in geochemically distinct parental melts during the assembly of the Skuggafjöll magma. The negative correlation may be accounted for by mixing of a CO_2-supersaturated depleted melt with a CO_2 degassed enriched melt shortly before eruption.
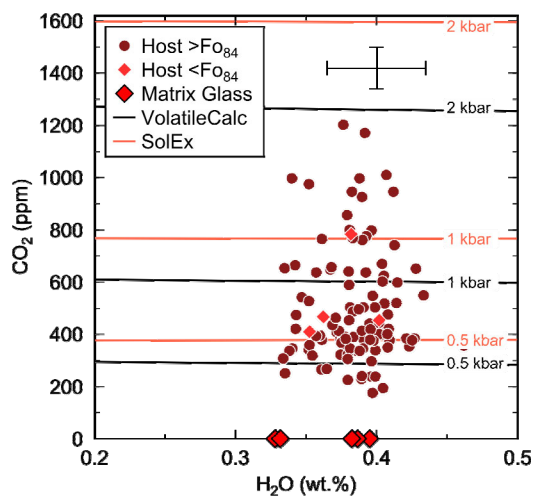
Figure 2 H_2O and CO_2 contents of Skuggafjöll melt inclusions. Isobars from two parameterisations of H_2O-CO_2 equilibrium are shown.
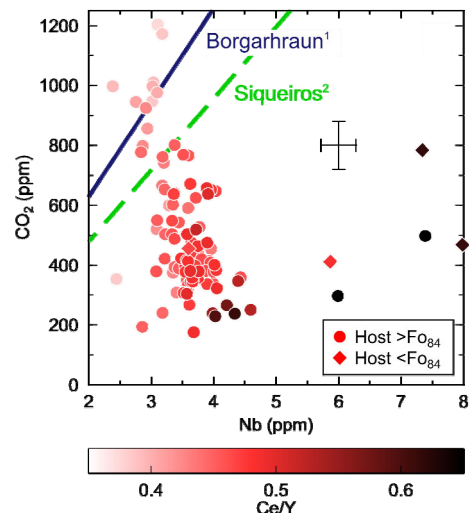
Figure 4 Negative correlation of CO_2 with Nb. High CO_2 and CO_2/Nb inclusions are associated with depleted, low Ce/Y. CO_2/Nb from Iceland[1] and Siquerios[2] shown for comparison.

References

[1] Hauri E.H. et al. (2002) *AGU, Spring Meeting* **V51D-03**

[2] Saal A.E. et al. (2002) *Nature* **419**, 451-455

Volatile and Trace Element Variability of Siberian Traps Melts

[1]S. Novikova, [1]M. Edmonds,[1]J. Maclennan, [2]H. Svensen

[1]Department of Earth Sciences, University of Cambridge, Cambridge, CB2 3EQ, UK
[2]Center for Earth Evoluton and Dynamics, University of Oslo, Oslo, 1048 Blindern, Norway

Introduction

The Siberian Traps Large Igneous Province (Figure 1) is thought to have formed over 1 Ma at the end of the Permian, synchronous with the largest mass extinction in Earth's history, when >96% of all marine species disappeared. There remains much controversy as to the exact mechanism of the mass extinction. The source of volatiles is a crucial question as it determines the speciation of some volatile components, which then can lead to climate perturbation and ozone depletion to a different extent. Being the country rocks for the huge volumes of sills (about 800 000 km^3) evaporites and beds with organic-rich accumulations must have had a significant influence on the amount and composition of released gases. However, the contribution of magmatic volatiles is not well constrained. The objective of the current study was to test whether the melts of Siberian Traps are particularly rich in volatiles that could have such a dramatic environmental effect.

Figure 1. Schematic geological map of Tunguska Basin, Eastern Siberia (modified from [1]).
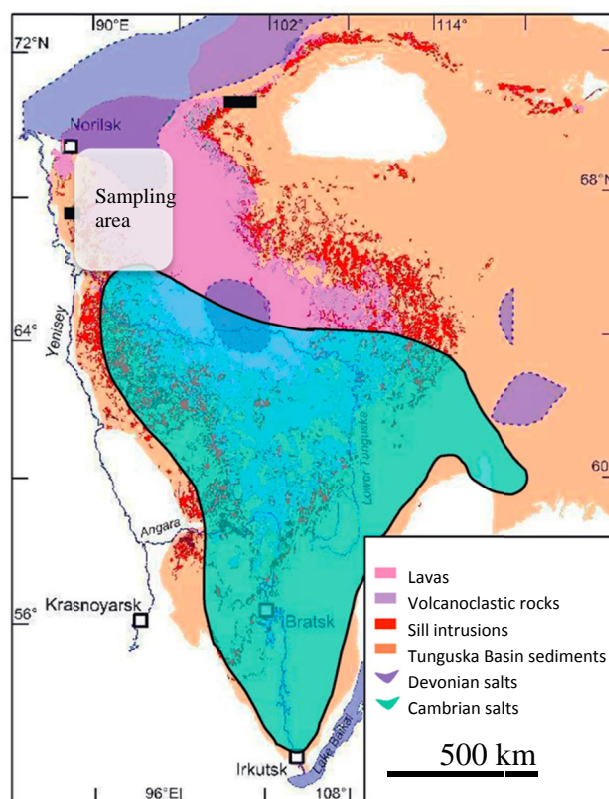
Results and Discussion

Analysed sills and lava flow samples south from Norilsk (Dupkin Lake region) were formed from evolved melts with a strong continental crust signature. Trace elements and volatiles in melt inclusions hosted by clinopyroxenes and olivines were measured by SIMS and then the same pits were analysed for major elements as well as for sulphur, chlorine and fluorine by EPMA in Cambridge.
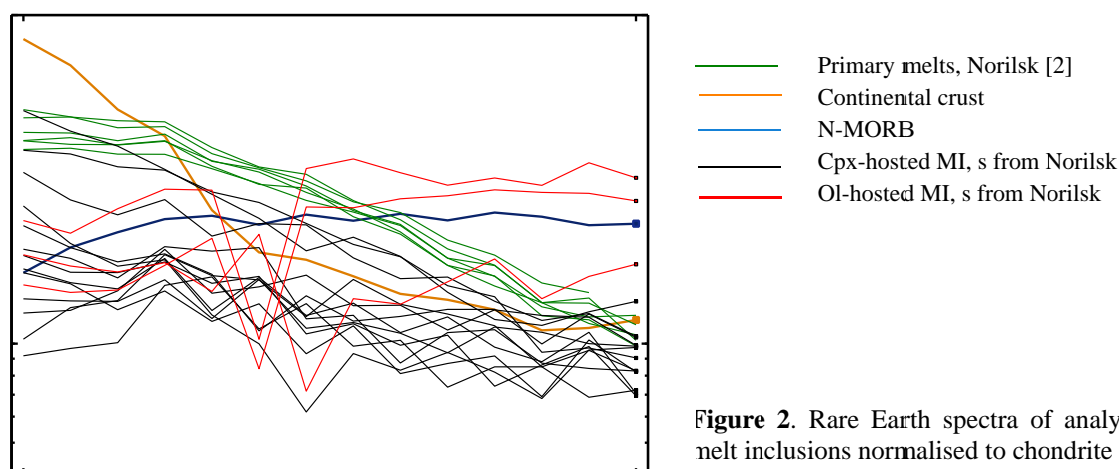
Figure 2. Rare Earth spectra of analysed melt inclusions normalised to chondrite

s revealed the variability of the melts (Figure 2). The rare earth elements patterns suggest a significant variability of evolved melts. Thus, La/Yb ratio for the inclusions in clinopyroxens varies from 1.4 to 5.6, whereas for the most primary melts of Siberian Traps it is within the interval from 4 to 5. Olivine-hosted melt inclusions are

characterised by La/Yb ratio of 0.4-1.6. Non-linear pattern is explained by analytical precision, which was up to 16% for Eu and close to 10% for heavy rare earth.

The current study presents the first F and CO_2 measurements for Siberian Traps melts. Carbon dioxide content of melt inclusions does not exceed 310 ppm suggesting extensive degassing. In order to assess the relative abundance of other volatiles the ratio of a particular volatile component to a trace element with same compatibility in the melt was considered.

Not only that both primary (red) and evolved (black) Siberian Traps melts are below sulphide saturation line, but they are also relatively poor in sulphur compare to MORB and Kilauea melts (Figure 3, left). In case of primary melts it indicates that sulphide saturation occurred after olivine crystallisation. The last suits of the intrusive sequence were already low in sulphur due to degassing and previous ore formation. F/Nd ratio varies from 0.1 to 73, whereas the one for Kilauea Iki melts is 17-32.
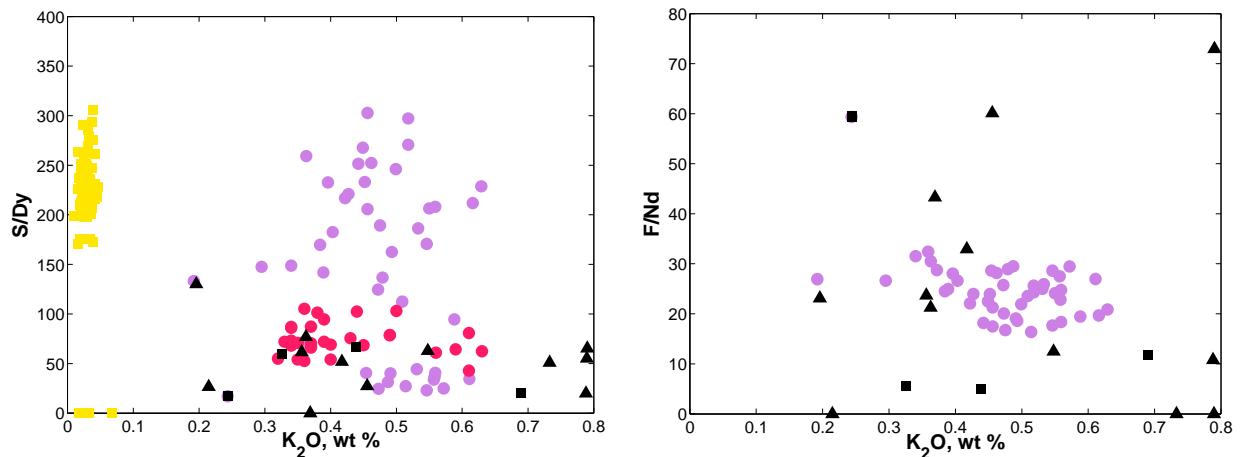
Figure 3. Sulphur-dysprosium ratio (left) and fluorine-niodimium ratio (right) vs potassium oxide: black – CPx (triangles) and Ol (circles) hosted MI; red circles – primary melts of Siberian Traps [2]; yellow square - Siquerious MORB [3]; lilac circles – Kilauea Iki [4].

Demonstrated volatile and trace elements variability requires more investigation. More ion probe analyses are planned to be done on the samples from the same region south from Norilsk aiming more detailed statistical analysis.

References

[1] G. Iacono-Marziano et al. (2012) Earth and Plenetary Science Letters **357-358**, 308-318.

[2] A.V. Sobolev et al. (2009) Petrology **17, 3**, 253-286.

[3] Saal et al. (2002) Nature, **419**, 451-455.

[4] I. Sides PhD Thesis, 2013

Evidence for Mixing and Degassing in the Deep Plumbing of Mt Etna, Sicily, from Melt Inclusions

L. Salem[1], M. Edmonds[1], J. Maclennan[1] & R. A. Corsaro[2]

[1]Department of Earth Sciences, Downing Street, University of Cambridge, Cambridge, CB2 3EQ, UK
[2]Instituto Nazionale di Geofisica e Vulcanologia, Sezione di Catania, Italy

Introduction and Background

The melts feeding Mt Etna are rich in volatiles and drive frequent, explosive eruptions that are a hazard to the local population. Understanding the volatile budget requires a detailed understanding of how melts ascend, differentiate and degas through the deep plumbing system. There have been many studies focusing on quantifying volatiles at Mt. Etna [e.g. 1, 2] and a single study focusing on trace element heterogeneity in melt inclusions [3]; few studies have attempted to link heterogeneity to volatiles. There are aspects of volatile behaviour that remain largely unconstrained at Etna: we have little understanding of the compositions of primary melts, and their degree of heterogeneity. This information is important to understand the geochemical characteristics of the mantle source. Understanding the length scales of heterogeneity may allow insight into the frequency of primitive injections triggering eruptions on annual and decadal cycles.

Aims & Strategy

To establish the composition of primary melts and to deconvolve the effects of assimilation, degassing and fractionation on melt composition with respect to volatiles [1, 2, 3, 4]. To understand better the links between degassing and eruption style. We use geochemical data to unravel source melt heterogeneity from processes affecting the melt during ascent and storage (fractionation, degassing and assimilation).

Methods

We focus here on the primitive 1669 eruption, the largest eruption of Etna in historical times. It began with violent explosive activity and developed into a destructive effusive event lasting four months. We collected samples from the main cinder cone at Monti Rossi, SE Etna flank and analysed olivine-hosted glassy melt inclusions for volatiles and a full suite of trace elements using 4f-ion probe (SIMS) in Edinburgh, and major elements using electron microprobe (EPMA) in Cambridge. We analysed CO_2 in shrinkage bubbles within the glassy inclusions using Raman Spectroscopy in Cambridge.
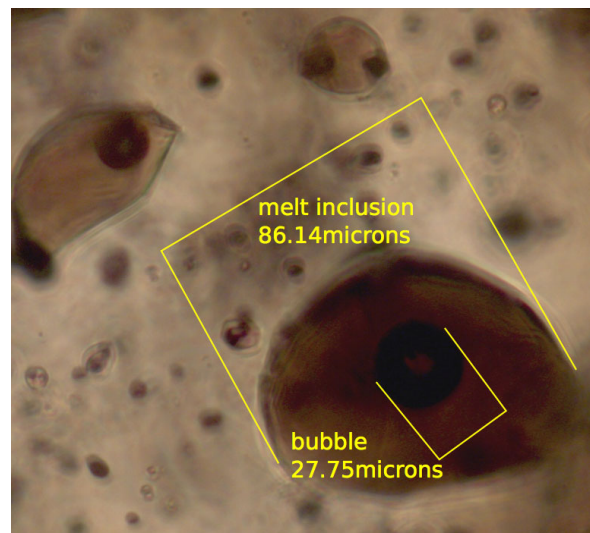
Figure 1: Reflected light image of olivine hosted melt inclusion with spherical shrinkage bubble.

Results

Trace and major elements: The analysed melt inclusions show extensive heterogeneity in terms of trace elements, which might indicate mixing of compositionally distinct melts and perhaps assimilation of crustal carbonate material. There is a large range in trace element ratios (La/Yb 15-55), with no relation to Fo content, unlike Iceland. The correlation between the volatiles carbon and sulphur with strontium might suggest a fraction of the volatiles are sourced from crustal carbonate. We propose future work to model these mixing trends, including assimilated basement material.

Volatiles: H_2O, CO_2 and sulphur concentrations range up to 2.0 wt%, 1200 ppm and 1900 ppm respectively. H_2O/Ce is <150 in MI hosted by olivines with Fo_{73-75} mol%. CO_2/Nb is low, suggesting CO_2 has been subject to extensive degassing or sequestration into a shrinkage bubble. There is a relationship between "degree of enrichment" (LREE/HREE) and volatile content, which may indicate mixing. There is a substantial portion of CO_2 locked away in shrinkage bubbles, which has not previously been accounted for in volatile studies at Etna.

Future work

We will link geochemistry found in our analyses back to the surface gas emissions to gain a more complete understanding of the plumbing system and controls on activity, and how magma mixing relates to triggering explosive eruptions. We will compare the 1669 melt inclusions with analyses of olivine hosted melt inclusions from recent explosive eruptions (2000 & 2008) with known lava fountaining events. We want to quantify the volatile budget during lava fountaining events with a knowledge of trace and major element composition to unravel the extent of heterogeneity, magma mixing, fractionation and degassing in the deep plumbing system. Ultimately we would like to deconvolve the influence of source volatile budget, processing and degassing on the eruptive phenomena, such as lava fountaining seen and monitored at the surface of Mt. Etna.

Figure 2. Trace element plots, cross NE sample, circle SW sample

Figure 3: Volatile plots against trace elements and olivine Fo content.

References

[1] Spilliaert *et al.* (2006). J. Geophys. Res. **111**, B04203
[2] Collins *et al.* (2009). Geology **37**(6), 571-574
[3] Kamenetsky *et al.* (2007). Geology **35**, 255-258
[4] Metrich, N. & Wallace, P.J. 2008. Reviews in Mineralogy and Geochemistry **69**, 363-402

I.J. Sansom, J.R. Wheeley & I. Boomer

School of Geography, Earth and Environmental Sciences, Univ. of Birmingham, Birmingham B15 2TT

(page intentionally left blank)

The Development of Vein Networks in Gabbroic Rocks from the Mid-Atlantic Ridge

W.T.B. Smith[1], L.A. Kirstein[1] & J.C.M. De Hoog[1]

[1]School of GeoSciences, University of Edinburgh, Edinburgh EH9 3JW, UK

Scientific Report

The formation of oceanic core complexes (OCCs) is generally attributed to the formation of long-lived detachment faults within the oceanic crust adjacent to slow- to ultraslow-spreading centres. However, reported depths and models of the detachment root zones are debated; with both deep and shallow lithospheric root zones being postulated. A detailed petrographic and geochemical study of gabbroic samples recovered from an OCC at 5°S on the Mid-Atlantic Ridge was undertaken, with the one-day ionprobe time used to: (1) determine the origin of zircon within the samples using rare-earth-element (REE) chemistry; and (2) determine the temperatures at which the veins crystallised and last equilibrated by means of Ti-in quartz and Ti-in-zircon thermometry.

The zircon REE data indicate high La/Sm values and low La contents indicative of a magmatic origin for the grains. Ti determinations from the ion microprobe were used in a number of thermometers including Ti in quartz and Ti in zircon. Ti-in-quartz and Ti-in-zircon thermometry was conducted using the calibrations of [1] and [2], respectively.

The results helped to resolve distinct stages of metasomatism and hydrothermal alteration including: (1) Magmatic uralitisation (>750°C) resulting in the formation of high-Ti amphibole, due to the interaction of late-stage, interstitial, hydrous differentiates within the hypersolidus crystal mush of the gabbroic pluton; (2) Formation of hydrothermal, low-Ti, amphibole (<500°C) after magmatic amphibole and as a product of further uralitisation in response to the infiltration of seawater-derived hydrothermal fluids; (3) Low-temperature alteration (<350°C) associated with chloritisation and sericitisation in response to the pervasive infiltration of seawater-derived fluids. Hydrothermal alteration is limited to greenschist and zeolite facies conditions, which is inconsistent with conventional 'hot' detachment models, instead a 'cold' detachment model where the root of the detachment is at the base of a hydrothermal alteration front within the oceanic crust (300-450°C) is considered viable in this case.
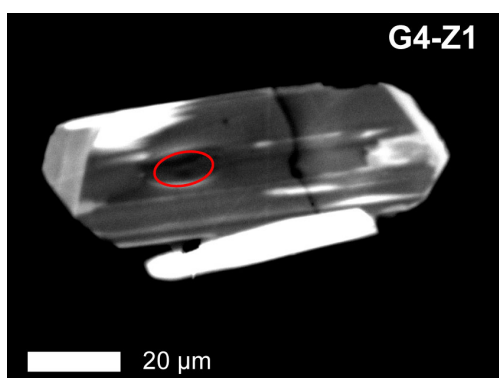
Figure 1. CL image of a zircon from a leucocratic vein. Red ellipse marks the location of the ionprobe spot.
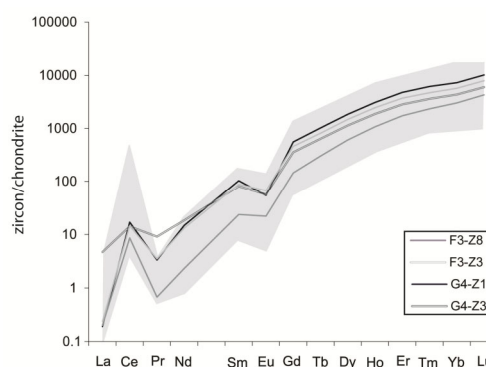
Figure 2. Chondrite-normalized REE patterns for zircons from the leucocratic veins. Low La and high Sm/La ratios are characteristic of magmatic zircons. Grey indicates compositional range of zircons from oceanic crust [3].

References

[1] J.B. Thomas et al. (2010) Contributions to Mineralogy and Petrology **160**, 743-759.
[2] E.B. Watson et al. (2006) Contributions to Mineralogy and Petrology **151**, 413-433.
[3] CB Grimes et al. (2009) Contributions to Mineralogy and Petrology **158**, 757-783.

(page intentionally left blank)

Generation and Preservation of Continental Crust in the Grenville Orogeny

Christopher J. Spencer[1]*, Peter A. Cawood[1], Chris J. Hawkesworth[1], Anthony R. Prave[1], Nick M.W. Roberts[2], Matthew S.A. Horstwood[2], Martin J. Whitehouse[3], EIMF[4]

[1]Department of Earth and Environmental Sciences, University of St Andrews, St Andrews, UK KY16 9AL
[2]NERC Isotope Geosciences Laboratory, British Geological Survey, Keyworth, Nottingham, NG12 5GG, UK
[3]Swedish Museum of Natural History and Nordic Center for Earth Evolution (NordCEE), Box 50 007, SE-104 05 Stockholm, Sweden
[4]Edinburgh Ion Microprobe Facility, University of Edinburgh, Edinburgh, EH9 3JW, UK

Abstract

Detrital zircons from modern sediments display an episodic temporal distribution of U-Pb crystallization ages forming a series of 'peaks' and 'troughs', which are interpreted to represent either periods of enhanced generation of granitic magma perhaps associated with mantle overturn and superplume events or preferential preservation of continental crust during global collisional orogenesis (Fig. 1).
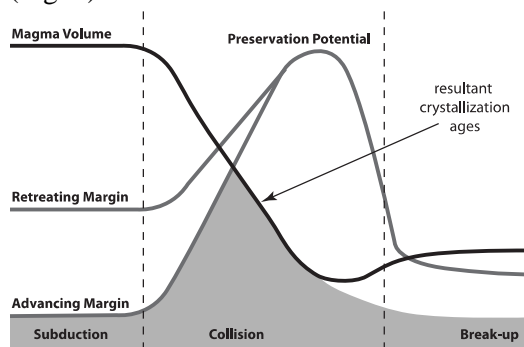
Figure 1: The volumes of magma generated (black line) and their likely preservation potential (grey line) vary through the three stages associated with the convergence, assembly, and breakup of a supercontinent [1]. Peaks in igneous crystallization ages that are preserved in the rock record (shaded area) reflect the balance between the magma volumes generated during the orogenic cycle and their respective preservation potential.

The close association of those peaks with the assembly of supercontinents implies a causal relationship between collisional orogenesis and the presence of zircon age peaks. Here these two end-member models (episodic periodicity of increased magmatism versus selective preservation during collisional orogenesis) are assessed using U-Pb, Hf, and O analysis of detrital zircons from sedimentary successions deposited during the ~1.3-1.1 Ga accretionary, ~1.1-0.9 Ga collisional, and < 0.9 Ga extensional collapse phases of the Grenville orogenic cycle in Labrador and Scotland (Fig. 2). The pre-collisional, accretionary stage provides a baseline of continental crust present prior to orogenesis and is dominated by Archean and Paleoproterozoic age peaks associated with pre-1300 Ma Laurentian geology. Strata deposited during the Grenville Orogeny display similar Archean and Paleoproterozoic detrital populations along with a series of broad muted peaks from ~1500 to 1100 Ma. However, post-collisional sedimentary successions display a dominant age peak between 1085 and 985 Ma, similar to that observed in modern North American river sediments.

Zircons within the post-orogenic sedimentary successions have progressively lower ε_{Hf} and higher $\partial^{18}O$ values post-1800 Ma until ~1200 Ma whereupon they have higher ε_{Hf} and $\partial^{18}O$ within the dominant 1085-985 Ma age peak. Furthermore, the Lu-Hf isotopic profile of the Grenville-related age peak is consistent with significant assimilation and contamination by older crustal material. The timing of this dominant age peak coincides with the peak of metamorphism and magmatism associated with the Grenville Orogeny, which is a typical collisional orogenic belt (Fig. 3).
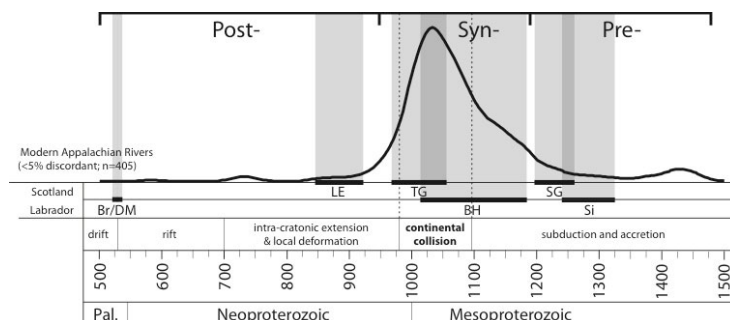
Figure 2: The age range of pre-, syn-, and post-orogenic sedimentary successions sampled in this study overlain by the zircon U-Pb age spectra. The vertical axis represents relative probability. Highlighted above the time scale are the stages of the Grenville orogenic cycle. Br: Bradore Formation; DM: Double Mer Formation; LE: Loch Eil Formation; TG: Torridon Group; BH: Battle Harbour Psammite; SG: Sleat Group; Si: Siamarnekh Formation.
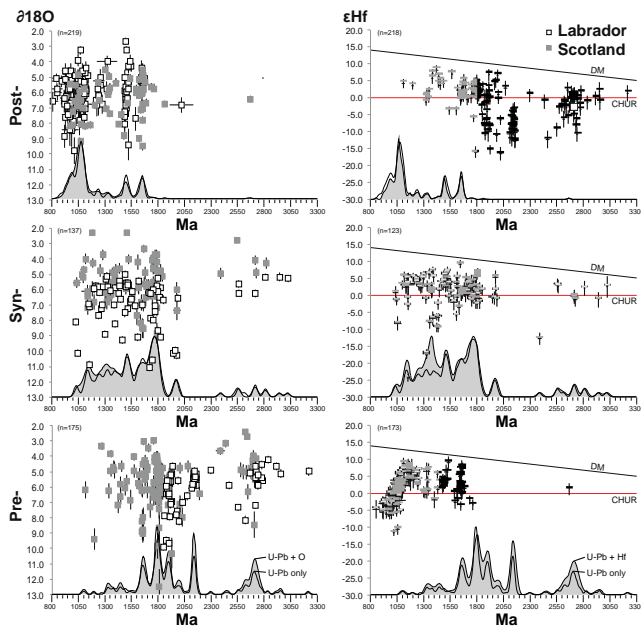
Figure 3: Left: $\partial^{18}O$ (‰ VSMOW) vs. U-Pb analyses of detrital zircons from the pre-, syn-, and post-orogenic sedimentary successions from Labrador and Scotland. Uncertainties are displayed as 2σ. Right: εHf(t) vs. U-Pb analyses of detrital zircons from the same. Uncertainties are displayed as 2σ. DM: depleted mantle; CHUR: Chondritic unfractionated reservoir.

The change from broad muted age peaks in the syn-orogenic strata to a single peak in the post-orogenic sedimentary successions and the modern river sediments implies a significant shift in provenance following continental collision. This temporal change in provenance highlights that the source(s), from which detrital zircons within syn-orogenic strata were derived, was no longer available during the later stages of the accretionary and collisional stages of the orogenic cycle. This may reflect either its tectonic burial, erosion, or possibly recycled into the mantle by tectonic erosion. During continental collision, the incorporated continental crust is isolated from crustal recycling processes operative at subduction margins. This tectonic isolation combined with sedimentary recycling likely controls the presence of the isotopic signature associated with the Grenville Orogeny in the modern Mississippi and Appalachian river sediments. These results imply that zircon age peaks, which developed in conjunction with supercontinents, are the product of selective crustal preservation during collisional orogenesis (Fig. 4).
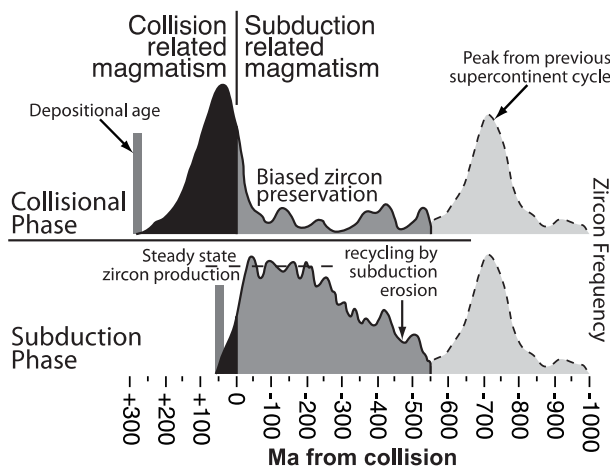
Figure 4: The idealized zircon age spectra during the subduction phase displays the age peak associated with the previous supercontinent cycle along with a broad plateau of ages representing steady-state zircon growth during subduction-related magmatism. Subduction erosion continually removes the oldest zircons associated with the phase of the orogenic cycle. This process continues until continental collision (and supercontinent assembly) continues to remove the previously formed subduction zone-derived zircons. Zircons that are formed during collision-related magmatism are preserved within the interior of the recently collided continents thus protecting it from future subduction erosion. This allows for significant temporal perpetuation of the age peak associated with the collisional orogenesis and the assembly of a supercontinent.

References
[1] C.J Hawkesworth et al. (2009) Science **323**, 49-50

Understanding Electron Beam-Induced Volatile Migration in the Apatite Crystal Lattice

M.J. Stock[1], M.C.S. Humphreys[1,2], V.C. Smith[3] & D.M. Pyle[1]

[1]Department of Earth Sciences, University of Oxford, Oxford OX1 3AN, UK
[2]Department of Earth Sciences, Durham University, Durham DH1 3LE, UK
[3]Research Labs for Archaeology and the History of Arts, University of Oxford, Oxford OX1 3QY, UK

Introduction

Apatite is a common accessory mineral in igneous rocks. It is present in many different volcanic and ore-forming systems, principally due to the low solubility of phosphorus in natural melts and fluids. Importantly, the apatite crystal lattice is capable of incorporating a wide range of volatile species which are present in magmatic systems, including OH^-, CO_3^{2-}, SO_4^{2-}, F^- and Cl^-. Most of these volatiles are accommodated as monovalent anions (principally F^-, Cl^-, OH^-) within a hexagonal channel site, which extends along the c-axis of the apatite crystal lattice.

Electron probe microanalysis (EPMA) represents the cheapest, easiest and most commonly accessible technique for apatite volatile analysis. It allows direct measurement of F, Cl and S concentrations on micro-meter length-scales and estimation of OH^- concentrations by difference. However, EPMA apatite analysis suffers from well-documented analytical difficulties, the most concerning of which is a significant anisotropic, time-dependent variation in halogen x-ray count rates during prolonged electron beam exposure [1]. Despite recent work aimed at optimisation of the EPMA operating procedure, to attain accurate apatite volatile analyses [2], the fundamental mechanisms responsible for the variability in x-ray count rates remain unclear.

In this study our aim was to constrain directly the processes responsible for the temporal variability in apatite halogen x-ray count rates observed during EPMA. This included determination of both the driving forces that cause halogen redistribution within apatite samples and the mechanisms by which halogens migrate within the crystal structure. The results are important for improving the quality of future EPMA, SIMS and fission track analyses. Furthermore, an improved understanding of halogen migration in apatite is important in geological and biological studies, as well as in investigations of the potential use of phosphate minerals in nuclear waste disposal.

Methods

In order to observe the electron beam-induced alteration to the halogen distribution within apatite crystals, we performed a series of two-stage experiments. In the first stage apatite samples were irradiated using a JEOL 8600 4-spectrometer electron microprobe. A 5 µm beam diameter and 15 nA current were maintained throughout. The accelerating voltage was varied from 10-15 kV. Samples of fluorapatite and chlorapatite were irradiated, in order to assess the effect of changing apatite composition. Fluorapatite samples were irradiated both parallel and perpendicular to c-axis, in order to investigate the anisotropy of the response to electron beam irradiation. Crystals were irradiated for different lengths of time, between 10 and 540 seconds, to examine the temporal variations in the halogen x-ray count rates.

In the second part of the experiment, SIMS depth profiles were created through the electron beam-irradiated areas. Prior to analysis of irradiated spots, non-irradiated areas of each apatite crystal were analysed to provide a baseline depth profile. Then for each irradiated point the SIMS beam was manually aimed on the EPMA spot, in order to sputter continuously down through the irradiated volume, thus collecting depth information about the altered apatite chemistry. SIMS profile points and EPMA spots were aligned using polishing scratches left on the sample surface during sample preparation. A 3D scanning NanoFocus confocal optical profiler
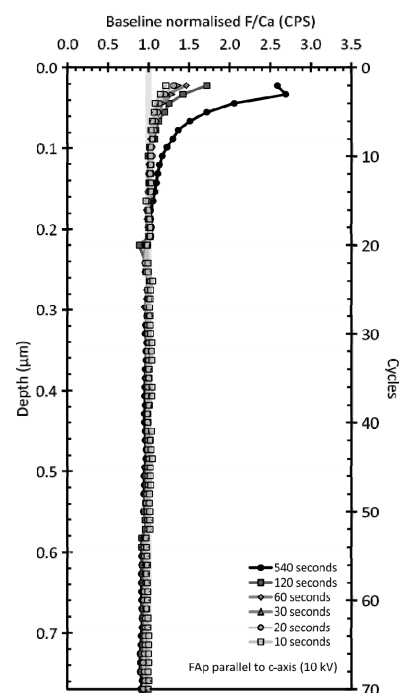
Figure 1. F/Ca depth profiles in fluorapatite irradiated parallel to c-axis.

was used to convert the raw number of SIMS counting cycles to pit depth and hence calculate the depth of each SIMS profile.

Results

Fluorapatite crystals, irradiated parallel to c-axis, show enrichment in F and Cl above baseline values within ~0.1 µm of the sample surface (fig.1). The degree of enrichment increases on initial electron beam exposure, before reaching a maximum and subsequently decreasing. This trend follows the x-ray count rate variability observed in EPMA time scans (fig.2). The enrichment rate and the timing of the decrease in the degree of surface enrichment are dependent on the electron beam operating conditions. Under identical EPMA operating conditions, where the incident electron beam is oriented perpendicular to the apatite c-axis, F and Cl x-ray count rates remain constant, with no sign of surface enrichment through 360 seconds of electron beam irradiation. Similarly, under these electron beam conditions no surficial halogen enrichment is seen in chlorapatite crystals irradiated parallel to c-axis.
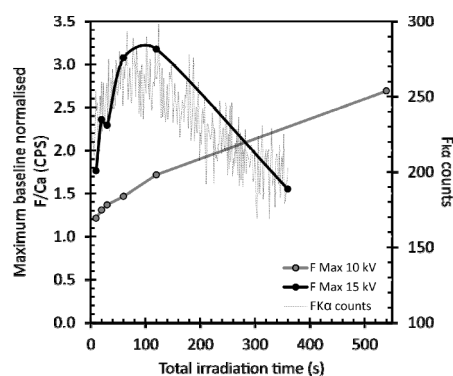
Figure 2. Maximum F concentration in depth profiles of irradiated FAp parallel to c-axis under different electron beam conditions (solid lines). EPMA time scan is shown by the black dashed line.

Discussion

During irradiation, electrons are implanted from the electron beam, generating an electric field within the sample. Furthermore, electron-matter interactions cause sample heating, with a steep thermal gradient down from the sample surface. In an insulating medium, such as apatite, these effects are localised within the electron probe interaction volume.

The observed surficial halogen enrichment can be explained by migration of anions away from the centre of charge build-up, which relates to the depth of maximum electron deposition. Apatite is more conductive at higher temperatures and migration is facilitated by the beam-induced heating. With prolonged beam exposure apatite crystals break down, depleting the surface region. Given the degree of enrichment at the sample surface, halogens are unlikely to have migrated into pre-existing vacancies. Instead, we believe that migration occurs through metastable interstitial sites.

The halogen diffusion coefficient is two orders of magnitude greater parallel to the crystallographic a-axis than in the c-axis direction [3]. Our data confirm that, under normal EPMA operating conditions, the effects of electron beam exposure are insufficient to induce migration in this direction. Similarly, the SIMS data indicate that migration is inhibited in Cl-rich apatites, which we ascribe to alteration to the c-axis channel caused by the transition between fluorapatite and chlorapatite crystal structure.

References

[1] J. Stormer et al. (1993) American Mineralogist **78**, 641-648
[2] B. Goldoff (2012) American Mineralogist **97**, 1103-1115
[3] J. Brenan (1993) Chemical Geology, **110**, 195-210

Oxygen Isotope Discrimination between Crustal and Mantle Sources of Primitive Low-Zr/Y and High-Zr/Y Icelandic Olivines

M. Thirlwall[1] & C. Manning[1]

[1]Department of Earth Sciences, Royal Holloway University of London, Egham, Surrey TW20 0EX, UK

Background

The unusually low $\delta^{18}O$ values of Icelandic magmas have usually been interpreted to be the result of assimilation of hydrothermally altered Icelandic crust. However, a correlation between $\delta^{18}O$ in Reykjanes Ridge olivines and host rock $^{143}Nd/^{144}Nd$ cannot be explained by contamination and suggests that there exists a low-$^{143}Nd/^{144}Nd$ Icelandic mantle source with $\delta^{18}O$ less than +4.2‰[1]. The origin of such a mantle source is not easily explained, however. SIMS $\delta^{18}O$ for olivines from the 1783 Laki eruption show a large range (+5.2 to +2.5‰) interpreted to be a result of contamination [2], suggesting that the laser fluorination (LF) olivine $\delta^{18}O$ data reported by [1] may represent mixtures of olivines with variable $\delta^{18}O$. A preliminary SIMS $\delta^{18}O$ study at Nancy of olivines from a sample reported by [1] yield a range in $\delta^{18}O$ from +2.9 to +4.6‰ (means of 4 spots in 5 separate grains) also suggestive of contamination. However, these grains showed almost no variation in %Fo, unlike those at Laki [2]. It is clear that relationships between olivine chemistry and in situ $\delta^{18}O$ should be the key to unravelling the relative effects of mantle $\delta^{18}O$ heterogeneity and crustal contamination in Icelandic magmas.

We have developed a new LA-ICP-MS technique at Royal Holloway that permits analysis of Sr, Zr, Y in olivine at ~1ppb detection limits, and have shown that these, and Ti contents, correlate with the chemistry of hosted melt inclusions. We have characterized a large number of megacryst olivines from Icelandic lavas and have demonstrated that many samples show heterogeneity in olivine Zr/Y that must reflect crystallization from magmas with variable Zr/Y and hence variable LREE enrichment and $^{143}Nd/^{144}Nd$. We selected olivine grains with the widest possible range of Fo content and Zr/Y in each sample for $\delta^{18}O$ analysis using the NERC Ion Probe facility.

Results

Most olivines analysed were $Fo_{>80}$. Measured $\delta^{18}O$ on Reykjanes Ridge Fo_{80} olivines with LF $\delta^{18}O$ = +5.2‰ were on most days indistinguishable from the $Fo_{90.3}$ in-house standard suggesting that the in-house fayalite standard may over-estimate the mass fractionation effect related to Fo content. All data discussed are means of 6 adjacent spots, with standard deviation of these mostly in the range 0.2-0.35, and 1sd on 6 is used as error bars on the diagrams.

1) $\delta^{18}O$ heterogeneity in low-$\delta^{18}O$ samples
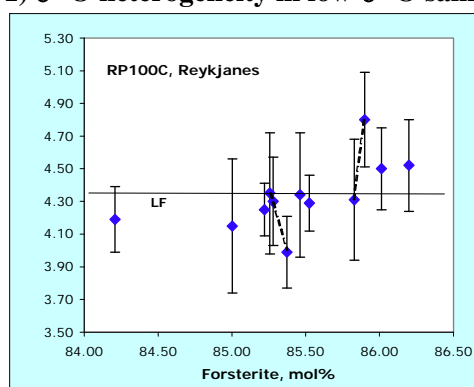
We analysed several key samples with low olivine LF $\delta^{18}O$ reported by [1], and unpublished, to investigate if similar in-sample heterogeneity exists as reported by [2] from Laki. This figure presents results from 9 grains of the same sample studied in Nancy. The two grains with $\delta^{18}O$ outside uncertainty of the LF value were re-analysed in the same analytical session, with the re-analyses shown by dashed tie-lines. There is no evidence of the scale of heterogeneity implied by the Nancy analyses, despite analysis of the most compositionally extreme grains from a population of 31. Similar results have been obtained on olivines from two other Reykjanes Peninsula samples with low LF $\delta^{18}O$. These yield $\delta^{18}O$ = +4.51±0.23‰ (2sd, 9 SIMS analyses; +4.26 by LF) and +4.56±0.23‰ (N=8, +4.43 by LF), although in the latter sample there is an unusual grain with 50% lower Ti and Y contents that yields $\delta^{18}O_{SIMS}$= +5.21±0.31‰ (1sd). This grain is intermediate in Fo, and cannot have grown from a magma with the high Ti and Y contents of its host, so provides no evidence that the lower $\delta^{18}O$ values

in the remaining olivines are the result of contamination. The sample with lowest $\delta^{18}O$ on the Reykjanes Ridge also has homogeneous olivines ($\delta^{18}O_{SIMS}$ = +4.60±0.18‰, 2sd, N=7 cf. +4.47 LF).

I320 Laki olivines (Forsterite vs δ¹⁸O)
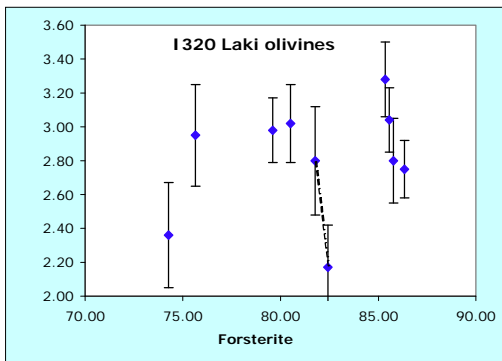
We have also analysed olivines from a postglacial Grímsvötn flow located within the Laki region. These, like the Laki samples of [2], shows a wide range in Fo (74-86%), and very different from typical Reykjanes Peninsula olivines, where individual lavas show limited Fo ranges. The adjacent diagram demonstrates that very low $\delta^{18}O$ is present over the full range of Fo. Two grains with significantly lower $\delta^{18}O$ were analysed, but re-analysis of one, in the same part of the grain, in the same analytical session, yielded $\delta^{18}O$ comparable to other grains. Olivines with >~87% Fo are not found in Icelandic rift zone lavas, with the exception of small volume lavas that are ultra-depleted in incompatible elements. These relatively primitive Fo_{86} olivines with $\delta^{18}O$ = +2.9‰ are very difficult to explain by contamination processes.

2) "Normal"-$\delta^{18}O$ samples

In the Reykjanes Peninsula, the only lavas to have olivine $\delta^{18}O$ by LF close to normal mantle values

RP3 Reykjanes Peninsula (δ¹⁸O plot, RP3 and RP95C)

are the ultra-depleted lavas referred to above[1]. We have analysed olivines by SIMS from three such samples. $Fo_{89.3-90.6}$ olivines in one of these with $\delta^{18}O_{LF}$ = +5.10 yield SIMS data averaging +4.97±0.35‰ (2sd on 7). There is a hint of a positive correlation between SIMS $\delta^{18}O$ and olivine Zr/Y and Ti contents (RP95C). Sample RP3 shows wide variation in olivine-hosted melt inclusion chemistry and shows rather wider variation in SIMS olivine $\delta^{18}O$ that appears to correlate with olivine Zr/Y, despite a narrow range in Fo of 89.3-89.8%. The higher olivine Zr/Y ratios are not in equilibrium with the very low host lava Zr/Y, and resemble Zr/Y and $\delta^{18}O$ in olivines from the dominant low-$\delta^{18}O$ incompatible-element-enriched magmas in the area. Since all these olivines have higher Fo than found in the latter lavas, it might be thought that this relationship indicates mixing between low- $\delta^{18}O$ incompatible-element enriched melts and high-$\delta^{18}O$ depleted melts in the melting column, but the relationship could equally be explained by incorporation of crustal xenocrysts, a hypothesis supported by the occurrence of plagioclase xenocrysts in this flow. A third incompatible-element-depleted lava studied contains partially disaggregated gabbro xenoliths. Fo_{91-84} olivines in this sample also show decreasing $\delta^{18}O$ with increasing Zr/Y, and decreasing Fo, over a >1‰ range in $\delta^{18}O$. This again supports a crustal origin for $\delta^{18}O$ variation in incompatible-element-depleted lavas.

Conclusions

Within the resolution of the SIMS data, we see very limited evidence for heterogeneity in olivine $\delta^{18}O$ in low-$\delta^{18}O$, incompatible-element-enriched lavas. In contrast we observe heterogeneity in higher-$\delta^{18}O$, incompatible-element-depleted lavas that contain plagioclase derived from crustal xenoliths, and this heterogeneity is linked to Zr/Y ratios in olivine. While it is much easier to observe contamination effects in the depleted lavas because of strong contrasts between them and dominant crustal materials, the presence of low-$\delta^{18}O$ olivine at >Fo_{86} in several incompatible-element enriched lavas clearly supports a mantle origin for this low $\delta^{18}O$.

References

[1] M.F. Thirlwall et al. (2006) Geochim. Cosmochim. Acta **70**, 993
[2] I. Bindeman et al. (2008) Geochim. Cosmochim. Acta **72**, 4397